

Dual-ligand fluorescence microscopy enables chronological and spatial histological assignment of distinct amyloid- β deposits

Received for publication, August 14, 2024, and in revised form, October 25, 2024. Published, Papers in Press, November 29, 2024.

<https://doi.org/10.1016/j.jbc.2024.108032>

Therése Klingstedt¹, Hamid Shirani¹, Farjana Parvin¹ , Sofie Nyström¹, Per Hammarström¹, Caroline Graff², Martin Ingelsson^{3,4,5} , Ruben Vidal⁶ , Bernardino Ghetti⁶, Dag Sehlin⁵ , Stina Syvänen⁵, and K. Peter. R. Nilsson^{1,*} 

From the ¹Department of Physics, Chemistry and Biology, Linköping University, Linköping, Sweden; ²Department of Neurobiology, Care Sciences and Society, Karolinska Institute, Stockholm, Sweden; ³Krembil Brain Institute, University Health Network, Toronto, Ontario, Canada; ⁴Tanz Centre for Research in Neurodegenerative Diseases, Department of Medicine and Laboratory Medicine & Pathobiology, University of Toronto, Toronto, Ontario, Canada; ⁵Molecular Geriatrics, Department of Public Health and Caring Sciences, Uppsala University, Uppsala, Sweden; ⁶Department of Pathology and Laboratory Medicine, Indiana University School of Medicine, Indianapolis, Indiana, USA

Reviewed by members of the JBC Editorial Board. Edited by Elizabeth J. Coulson

Different types of deposits comprised of amyloid- β (A β) peptides are one of the pathological hallmarks of Alzheimer's disease (AD) and novel methods that enable identification of a diversity of A β deposits during the AD continuum are essential for understanding the role of these aggregates during the pathogenesis. Herein, different combinations of five fluorescent thiophene-based ligands were used for detection of A β deposits in brain tissue sections from transgenic mouse models with aggregated A β pathology, as well as brain tissue sections from patients affected by sporadic or dominantly inherited AD. When analyzing the sections with fluorescence microscopy, distinct ligand staining patterns related to the transgenic mouse model or to the age of the mice were observed. Likewise, specific staining patterns of different A β deposits were revealed for sporadic *versus* dominantly inherited AD, as well as for distinct brain regions in sporadic AD. Thus, by using dual-staining protocols with multiple combinations of fluorescent ligands, a chronological and spatial histological designation of different A β deposits could be achieved. This study demonstrates the potential of our approach for resolving the role and presence of distinct A β aggregates during the AD continuum and pinpoints the necessity of using multiple ligands to obtain an accurate assignment of different A β deposits in the neuropathological evaluation of AD, as well as when evaluating therapeutic strategies targeting A β aggregates.

More than 100 years ago, abnormal brain deposits were identified as the essential neuropathological features of Alzheimer's disease (AD) (1). During the 1980s it was shown that the main components of these extracellular plaques and intracellular tangles were the amyloid- β (A β) peptide and the tau protein, respectively (2–4). The deposits of A β are mainly found in the brain parenchyma and in the cerebral blood

vessels, where different A β peptide species can be found. A β 1-42 is the most abundant peptide in parenchymal deposits, whereas blood vessel deposits are enriched in A β 1-40 (5–10). Structural studies of *in vitro* generated A β filaments have revealed a conformational heterogeneity (11–15). Likewise, A β filaments derived from seeded fibril growth using brain extract from AD patients with different disease phenotypes or distinct clinical subtypes have shown a structural variation when analyzed by solid state nuclear magnetic resonance (16, 17). Lately, cryo-EM studies of brain derived A β filaments have revealed the existence of various A β folds (18–23). Parenchymal A β 1-42 filaments extracted from AD brains showed two different filament types (19). The type I filament was found to be more prevalent in individuals with sporadic AD (sAD), whereas the type II filament was more pronounced in individuals with dominantly inherited AD (diAD). Alternative A β folds have also been observed for A β filaments derived from patients with the Arctic (APP E693G) mutation (20), as well as for A β 1-40 filaments in meningeal deposits (18, 21). Moreover, a variety of A β folds have been observed by cryo-EM when analyzing A β fibrils isolated from different transgenic mouse models displaying aggregated A β pathology (19, 20, 22). Overall, cryo-EM studies have demonstrated a variation of A β folds, which in combination with their post-translational modifications most likely explains the different types of A β deposits found in AD. Thus, novel methods that enable identification of a diversity of A β deposits during the AD continuum are essential for a more precise neuropathological diagnosis, as well as for understanding the role of these species during the pathogenesis.

From a histological perspective, A β deposits are routinely identified using immunohistochemistry, and a variety of different fluorescent amyloid ligands have also been presented (24). However, antibodies mainly identify the total amount of A β , and a variety of A β deposits might go undetected by conventional amyloid ligands. Carbon-11 labeled Pittsburgh

* For correspondence: K. Peter. R. Nilsson, peter.r.nilsson@liu.se.

Chronological and spatial assignment of amyloid- β deposits

compound-B ($[^{11}\text{C}]\text{PiB}$), the first ligand to be used clinically as a PET tracer for imaging of A β deposits (25), has shown poor binding to A β deposits in certain brain regions and reduced binding to brain homogenates despite evidence of an overall high A β load (26–28), as well as a limited ability to detect cotton wool plaques (CWPs), a certain type of A β deposits found in cases of diAD associated with presenilin-1 (*PSEN1*) mutations (29–31). Thus, neither immunohistochemistry nor the use of a single ligand can result in an accurate histological assignment of diverse aggregated A β deposits. In this regard, staining protocols using multiple ligands, or hyperspectral analysis with a single ligand, have been used for optical assignment of different A β deposits in brain tissue sections from transgenic mouse models or patients diagnosed with sAD or diAD (32–41). These studies have revealed a variation of A β aggregates in brain tissue sections from transgenic mouse models (32, 33, 36, 38, 40, 41), as well as the existence of different types of A β deposits in human AD brain tissue sections (33–38, 40). However, many of these previously reported approaches involved ligands with overlapping photophysical characteristics and competitive binding modes, as well as the need for advanced microscopy systems or complex data analysis.

In this work, we have applied several dual-staining protocols comprised of combinations of five previously reported thiophene-based ligands denoted HS-84 (42, 43), HS-169 (43), HS-259 (44), HS-276 (45), and HS-335 (44) (Figs. 1A and S1), for histological staining of A β deposits in brain tissue sections

from transgenic mouse models and individuals diagnosed with sAD or diAD. The ligands were selected and combined based on their photophysical characteristics with the aim of avoiding spectral overlap. In addition, these ligands have shown differential binding modes toward A β deposits (44–46). HS-84 and HS-169 share the same binding mode as the conventional amyloid ligand Congo red and thus detect both A β deposits and aggregated tau in AD brain tissue sections (frontal cortex) (43, 46). HS-259 has shown binding to tau aggregates and some A β deposits, such as cored A β plaques and cerebral amyloid angiopathy (CAA) lesions, whereas HS-276 and HS-335 have displayed a high selectivity toward A β aggregates (44, 45). Furthermore, it has previously been reported that HS-276 demonstrates a different binding mode than HS-169 (45). For HS-335, theoretical calculations have suggested two distinct binding modes on the A β filaments, corresponding to residues Gly 25 and Ser 26 or to Lys 16, Val 18, and Phe 20 (44). Herein, fluorescence molecular imaging of A β deposits in mouse brain tissue sections revealed specific ligand binding patterns for distinct mouse models, as well as for mice at different ages. Likewise, imaging of brain tissue sections (frontal cortex) from individuals with sAD or diAD displayed distinct ligand staining patterns of A β deposits. Furthermore, when examining different brain regions from individuals with sAD, various fluorescent patterns were observed for the distinct regions. Thus, the newly developed protocols for multiple-ligand fluorescence microscopy facilitated chronological and spatial assignment of A β deposits in

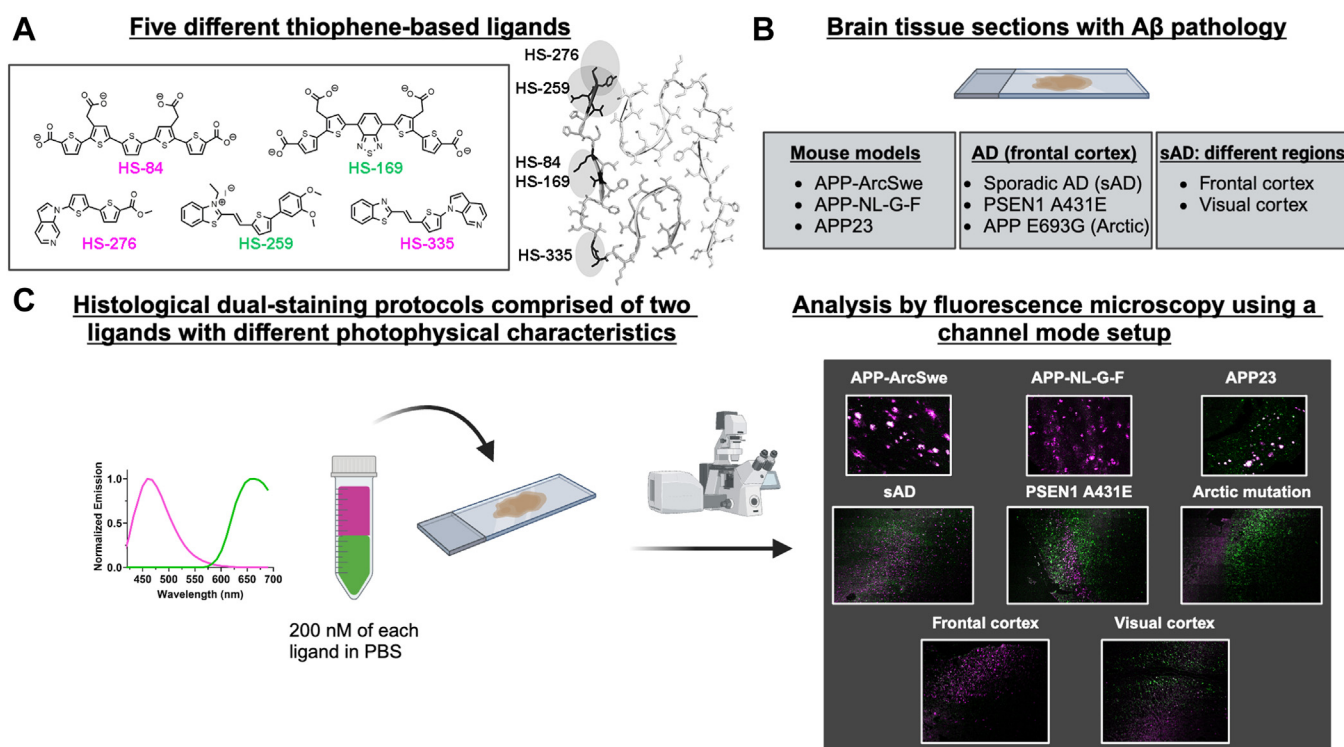


Figure 1. Schematic overview of the study. A, chemical structure of the five different thiophene-based ligands included in the study, as well as their suggestive binding mode to type I sporadic Alzheimer's disease filaments (PDB:7Q4B) (19) based on previous experimental and computational studies (44–46). B, the brain tissue sections with A β pathology included in the study. C, graphic presentation of the dual-staining protocols, as well as the analysis of the stained tissue sections with fluorescence microscopy. The figure was created with [BioRender.com](https://www.biorender.com). A β , amyloid- β ; PDB, protein data bank.

brain tissue sections from transgenic mouse models and individuals with AD. These findings support and emphasize the necessity of using several ligands to obtain a precise assignment of different A β deposits, and we foresee that our protocols can be used to achieve a greater understanding of the presence of distinct A β deposits during the AD continuum and aid in developing novel diagnostic tools for AD.

Results

Design of dual-staining protocols comprised of two ligands for histological assessment of A β deposits with fluorescence microscopy

To meet the criteria of having dual-staining protocols comprised of two ligands with tentative differential binding modes toward A β deposits (Fig. 1A), as well as separate photophysical properties enabling analysis by conventional confocal microscopy using a channel mode setup, the following six combinations of ligands were selected: HS-84/HS-259, HS-84/HS-169, HS-276/HS-259, HS-276/HS-169, HS-335/HS-259, and HS-335/HS-169. Given that the ligands might exhibit multiple concentration-dependent binding modes to A β aggregates, a concentration of 200 nM of each ligand in PBS (pH 7.4) was used to increase the probability of assessing the high-affinity binding mode for the respective ligand, as well as to avoid micelle formation or solubility issues of the ligands that might occur at higher concentrations. In addition, comparable concentrations (100 or 200 nM) have been used previously for identification of distinct protein aggregates in tissue samples with similar ligands (44, 45). A representation of the dual-staining protocols, as well as the analysis of the stained tissue sections with fluorescence microscopy, is shown in Figure 1.

Dual-ligand staining protocols comprised of HS-84/HS-259 or HS-335/HS-169 identify mouse model-specific and age-related A β deposits in brain tissue sections from APP mice

The dual-ligand protocols were initially evaluated by staining brain tissue sections from three different mouse models: amyloid-beta precursor protein (APP) transgenic mice with the Swedish mutation (APP23) (47), APP transgenic mice with the Swedish and Arctic mutations (APP_{ArcSwe}) (48), and knock-in mice that harbor the Swedish, Beyreuther/Iberian, and Arctic mutations in the APP gene (APP^{NL-G-F/NL-G-F}) (49). To investigate if the dual-staining protocols could assess an age-dependent variation of A β deposits, brain tissue sections from two different ages of each mouse model were evaluated (Table S1). When analyzing the HS-84/HS-259 stained brain tissue sections, different staining patterns could be observed depending on the mouse model, as well as the age of the mouse within the same model (Figs. 2 and S2–S4). In young APP_{ArcSwe} (7 months) and APP23 (8 months) mice, a nearly perfect colocalization between the ligands could be observed from the A β aggregates (Fig. 2, B and D), including the vascular deposits in the APP23 mice (Fig. 2D). In contrast, in old (22 months) APP_{ArcSwe} mice, fibrillar deposits that were only stained by HS-84 could be observed (Fig. 2C) and these

aggregates were also positive for the A β antibody 6E10 (Fig. S5), which has an epitope mapped to residues 5 to 7 of the A β peptide (50). In these mice, HS-259 fluorescence was only observed from larger HS-84 positive cored plaques and vascular deposits (Figs. 2C and S5). Hence, in the APP_{ArcSwe} mice, some age-dependent aggregated A β deposits that were only recognized by HS-84 were identified. A similar phenomenon was observed for the APP23 mice, but in contrast to the APP_{ArcSwe} model, deposits that were solely stained by HS-259 could be detected (Fig. 2E). Fluorescence from both ligands was clearly observed from large A β plaques, as well as from vascular deposits, whereas a larger amount of fibrillar deposits with a smaller size only displayed HS-259 staining (Fig. 2E) and these deposits were also labeled by the 6E10 antibody (Fig. S6). Thus, in old APP23 mice, A β deposits that were solely identified by HS-259 were presented. A similar age-dependent transition of A β deposits in APP23 mice has previously been observed when using a dual-staining protocol with a tetrameric oligothiophene, q-FTAA, and a heptameric oligothiophene, h-FTAA (32). When adding HS-259 to this set of ligands, a clear correlation between HS-259 and h-FTAA staining could be detected, whereas q-FTAA fluorescence was lacking from these aggregated species (Fig. S7). In young APP^{NL-G-F/NL-G-F} mice (4 months), HS-259 only labeled small cored A β deposits, whereas HS-84 fluorescence could be observed from the HS-259 positive cores as well as several additional fibrillar structures (Fig. 2F). This labeling pattern was even more pronounced in the old (18 months) APP^{NL-G-F/NL-G-F} mice, since HS-84 fluorescence was displayed from a larger number of A β aggregates compared to HS-259 (Fig. 2G). Fluorescence from HS-259 was only seen from vascular deposits and a small number of cored plaques, which were slightly larger than those observed in the young APP^{NL-G-F/NL-G-F} mice. The differential staining of the respective ligand in the old APP^{NL-G-F/NL-G-F} mice was also verified by the 6E10 antibody and HS-84 showed perfect colocalization with 6E10, whereas HS-259 only labeled a small number of 6E10 positive A β deposits (Fig. S8). Overall, the staining experiments showed that the dual-ligand staining protocol comprised of HS-84 and HS-259 could be used to assign a difference between A β deposits in the respective mouse model, since A β aggregates solely stained by HS-84 were observed in APP_{ArcSwe} and APP^{NL-G-F/NL-G-F} mice, whereas A β deposits merely stained by HS-259 were found in APP23 mice. In addition, age-related differential ligand staining patterns of A β aggregates were displayed within the APP_{ArcSwe} and APP23 mouse models (Fig. 2).

Distinct staining patterns for the different mouse models, as well as for different ages of the mice within the same model, could also be observed when analyzing brain tissue sections stained by a second combination of ligands, HS-335/HS-169 (Figs. 3 and S9–S11). In young APP_{ArcSwe} and APP23 mice, the A β deposits were stained by both ligands (Fig. 3, B and D), whereas in old APP_{ArcSwe} mice, HS-169 fluorescence was observed from the A β aggregates previously identified by HS-84, and the HS-335 staining pattern was comparable to HS-259 (Fig. 3C). Likewise, in old APP23 mice, HS-169 labeled

Chronological and spatial assignment of amyloid- β deposits

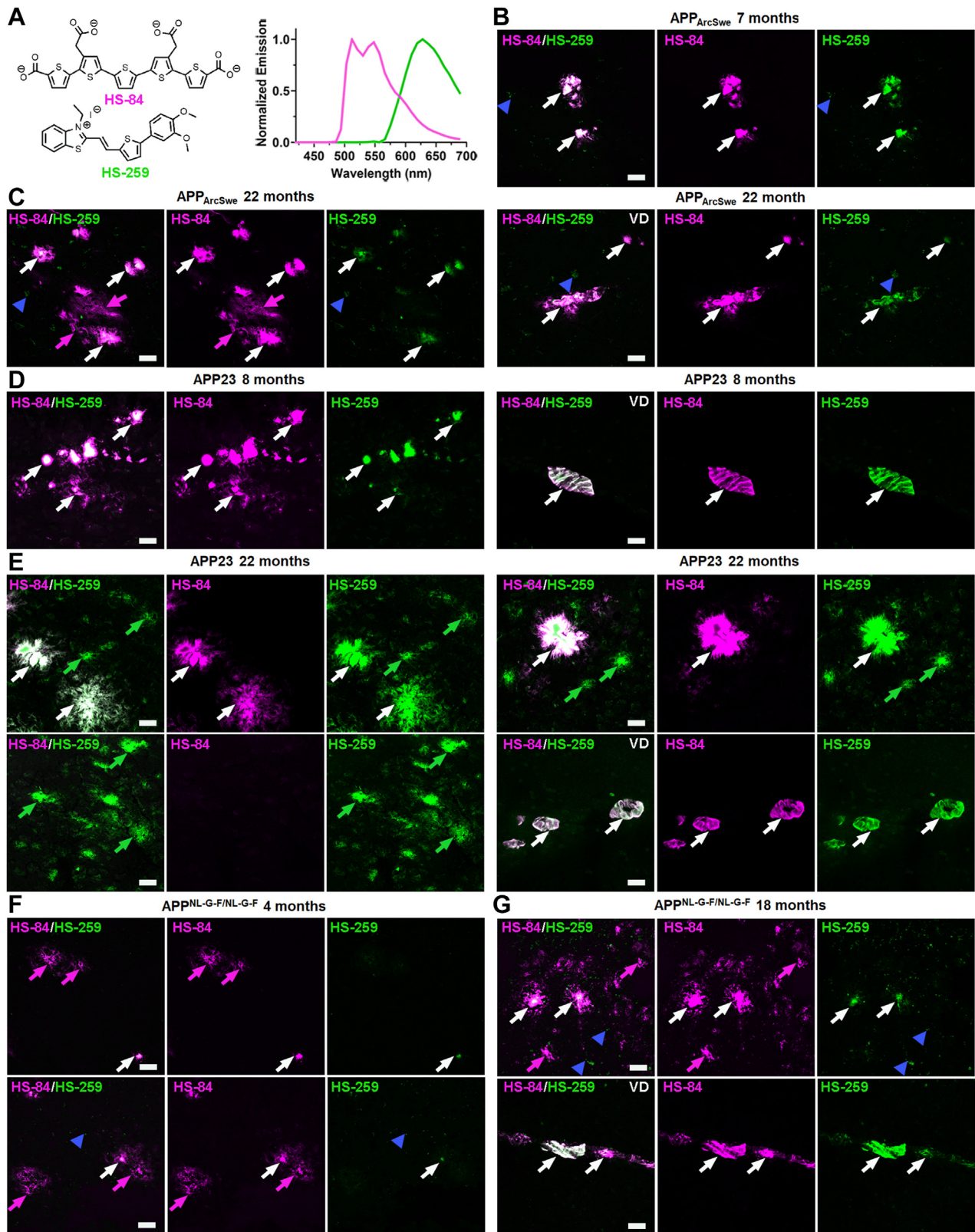


Figure 2. Dual-staining of brain tissue sections from APP mouse models with ligands HS-84 and HS-259. A, chemical structures and emission spectra of HS-84 (magenta) and HS-259 (green) bound to A β deposits. B–G, fluorescence images of brain tissue sections from 7 months (B) or 22 months (C) old APP_{ArcSwe} mice, 8 months (D) or 22 months (E) APP23 mice, and 4 months (F) or 18 months old (G) APP^{NL-G-F/NL-G-F} mice. A β aggregates stained by both ligands are indicated by white arrows, whereas A β aggregates only stained by HS-84 or HS-259 are highlighted with magenta arrows (HS-84) or green arrows (HS-259), respectively. Images showing vascular A β deposits (VD) are indicated with VD. All other images show parenchymal A β deposits. Autofluorescence from granular lipofuscin is indicated by blue arrow heads. The staining was performed using 200 nM of the respective ligand in phosphate buffered saline (PBS, pH 7.4). Scale bars represent 20 μ m. A β , amyloid- β ; APP, amyloid-beta precursor protein.

Chronological and spatial assignment of amyloid- β deposits

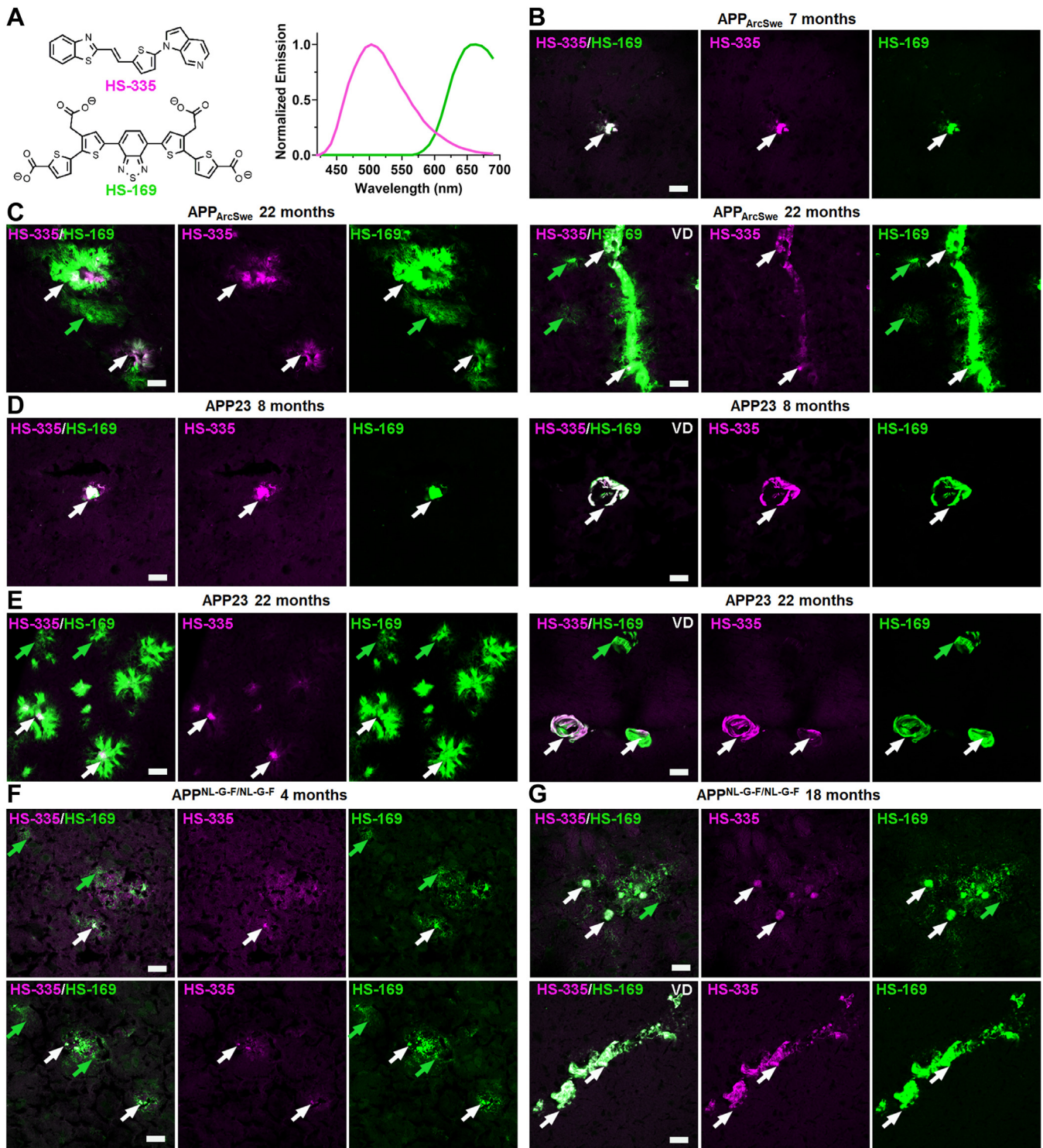


Figure 3. Dual-staining of brain tissue sections from APP mouse models with ligands HS-335 and HS-169. A, chemical structures and emission spectra of HS-335 (magenta) and HS-169 (green) bound to A β deposits. B–G, fluorescence images of brain tissue sections from 7 months (B) or 22 months (C) old APP_{ArcSwe} mice, 8 months (D) or 22 months (E) APP23 mice, and 4 months (F) or 18 months old (G) APP^{NL-G-F/NL-G-F} mice. A β aggregates stained by both ligands are indicated by white arrows, whereas A β aggregates only stained by HS-169 are highlighted with green arrows. Images showing vascular A β deposits (VD) are indicated with VD. All other images show parenchymal A β deposits. The staining was performed using 200 nM of the respective ligand in phosphate buffered saline (PBS, pH 7.4). Scale bars represent 20 μ m. A β , amyloid- β ; APP, amyloid-beta precursor protein.

similar A β aggregates as HS-84, but HS-335 fluorescence was only seen from the cores of these deposits (Fig. 3E). In addition, the HS-169 positive vascular deposits were only partially

labeled with HS-335 (Fig. 3E). In young and old APP^{NL-G-F/NL-G-F} mice, the smaller fibrillar A β aggregates previously identified by HS-84 were solely stained by HS-169. HS-335

Chronological and spatial assignment of amyloid- β deposits

fluorescence was only displayed from similar cored plaques as previously observed with HS-259 (Fig. 3, F and G). Hence, the fibrillar HS-84 positive A β aggregates in young and old APP^{NL-G-F/NL-G-F} mice, as well as in old APP_{ArcSwe} mice were only labeled with HS-169. Taken together, these staining experiments confirmed that dual-ligand staining protocols could be used to assign different types of A β deposits in the respective mouse model (APP_{ArcSwe}, APP23, and APP^{NL-G-F/NL-G-F}), as well as to reveal age-related A β aggregates within the same model (APP_{ArcSwe} and APP23).

Dual-ligand staining protocols comprised of HS-335/HS-259, HS-84/HS-169, HS-276/HS-259, or HS-276/HS-169 confirm the presence of mouse model-specific and age-related A β deposits in brain tissue sections from APP mice

To verify the results from the first two sets of ligand combinations, the four ligands were combined in a different fashion rendering staining protocols comprised of HS-335/HS-259 or HS-84/HS-169. When using HS-335/HS-259 (Figs. S12–S15), fluorescence from both ligands was displayed from the same types of A β deposits in the APP_{ArcSwe} mice (Fig. S12, B and C). Hence, in accordance with the results from the first two sets of ligand combinations (Figs. 2 and 3), staining of the fibrillar HS-84 and HS-169 positive A β aggregates in old APP_{ArcSwe} mice was lacking (Fig. S12C). Colocalization of the ligands was also observed for A β deposits in young APP23 mice (Fig. S12D). However, the previously identified HS-259 positive A β aggregates in old APP23 mice were again only stained by HS-259, whereas the vascular deposits displayed fluorescence from both ligands (Fig. S12E). In addition, as observed previously, HS-335 and HS-259 only stained small cored plaques and vascular deposits in APP^{NL-G-F/NL-G-F} mice (Fig. S12, F and G). The dual-staining protocol comprised of HS-84/HS-169 showed similar results as obtained for these ligands when used in combination with HS-259 or HS-335. In APP_{ArcSwe} and APP23 mice, A β aggregates displayed characteristic fluorescence from both ligands (Figs. S16–S19). In contrast, the fibrillar A β aggregates in APP^{NL-G-F/NL-G-F} mice that were solely stained by HS-84 or HS-169 when using these ligands in combination with HS-259 or HS-335, respectively, only displayed fluorescence from HS-84 (Fig. S16, F and G). HS-169 fluorescence was only observed from small cored plaques and vascular A β deposits. Thus, HS-84 and HS-169 could bind simultaneously to most A β deposits except for the fibrillar A β aggregates in young and old APP^{NL-G-F/NL-G-F} mice. For these deposits, the amount of accessible binding sites for the ligands might be restricted and since these ligands have similar binding modes, HS-84 displays a higher affinity than HS-169 toward these aggregates. As shown above, when used in combination with HS-335, HS-169 readily labeled these fibrillar A β aggregates (Fig. 3, F and G). In addition, when applying only HS-169 for staining, these fibrillar A β deposits were clearly labeled by this ligand (Fig. S20).

Dual-staining protocols with ligand HS-276 in combination with HS-169 or HS-259 were also used on mouse brain tissue sections. HS-169 and HS-259 displayed similar staining

patterns of A β deposits as when used in combination with HS-84 or HS-335 (Figs. S21–S28). Overlapping HS-276 fluorescence was observed from A β deposits in young APP_{ArcSwe} and young APP23 mice (Figs. S21, B and D, S25, B and D). However, for the A β deposits solely detected by HS-169 (Fig. S21C) or HS-259 (Fig. S25E) in old APP_{ArcSwe} or APP23 mice, respectively, fluorescence from HS-276 was lacking. In these older mice, HS-276 fluorescence was only observed from vascular A β deposits and some partially stained large cored A β plaques (Figs. S21, C and E, S25, C and E). A similar phenomenon was shown in APP^{NL-G-F/NL-G-F} mice, in which HS-276 only labeled small HS-169 and HS-259 positive cored plaques and vascular A β deposits (Figs. S21, F and G, S25, F and G). Hence, similar to the observations for HS-259 and HS-335, HS-276 fluorescence from the HS-169 and HS-84 positive fibrillar A β aggregates in APP^{NL-G-F/NL-G-F} mice was lacking. Overall, the histological analysis of brain tissue sections from different APP mouse models clearly showed that dual-staining protocols comprised of two different ligands can be used to assign distinct A β aggregates by fluorescence microscopy using an ordinary channel mode setup. Different ligand staining patterns were observed for each mouse model, and in two of the models, APP_{ArcSwe} and APP23, age-related A β deposits that were solely identified by one (HS-259 in APP23) or two ligands (HS-84 and HS-169 in APP_{ArcSwe}) could be observed (Fig. 4).

Dual-ligand staining protocols identify distinct A β deposits in brain tissue sections from individuals with sAD and diAD

Next, the same protocols were used to stain brain tissue sections (frontal cortex) from individuals with sAD (n = 3) and diAD. To represent the latter, cases (n = 3) from individuals with the *PSEN1 A431E* mutation (51–53) or the Arctic mutation (APP E693G) (n = 2) (54, 55) were selected, since these mutations are known to induce a variety of different A β deposits, such as CWP, that have alternative morphologies and different compositions of A β peptides than those observed in sAD (30, 56–58). When examining the sections stained by HS-276/HS-169, strikingly different staining patterns could be observed for the distinct cases of AD (Figs. 5 and S29). For sAD cases, weak HS-276 fluorescence was observed from CAA lesions in blood vessel walls (Fig. 5B), whereas intense HS-276 fluorescence was displayed from cored (Fig. 5C) and diffuse (Fig. 5D) A β plaques, as well as from A β deposits in the white matter (Fig. 5E). In contrast, HS-169 only stained CAA lesions (Fig. 5B), cored A β plaques (Fig. 5C) and tau aggregates, such as neurofibrillary tangles, dystrophic neurites, and neuropil threads (Fig. 5). Thus, these ligands recognized different A β deposits in sAD, and these observations agree with previous studies in which each individual ligand was used for staining of brain tissue sections (frontal cortex) from sAD cases (43, 45). In the *PSEN1 A431E* cases, a laminar staining pattern correlating to the fluorescence from the respective ligand could be observed (Figs. 5F and S29). Comparable to the sAD cases, aggregated tau pathology was only visualized by HS-169 fluorescence, whereas both ligands labeled CAA lesions

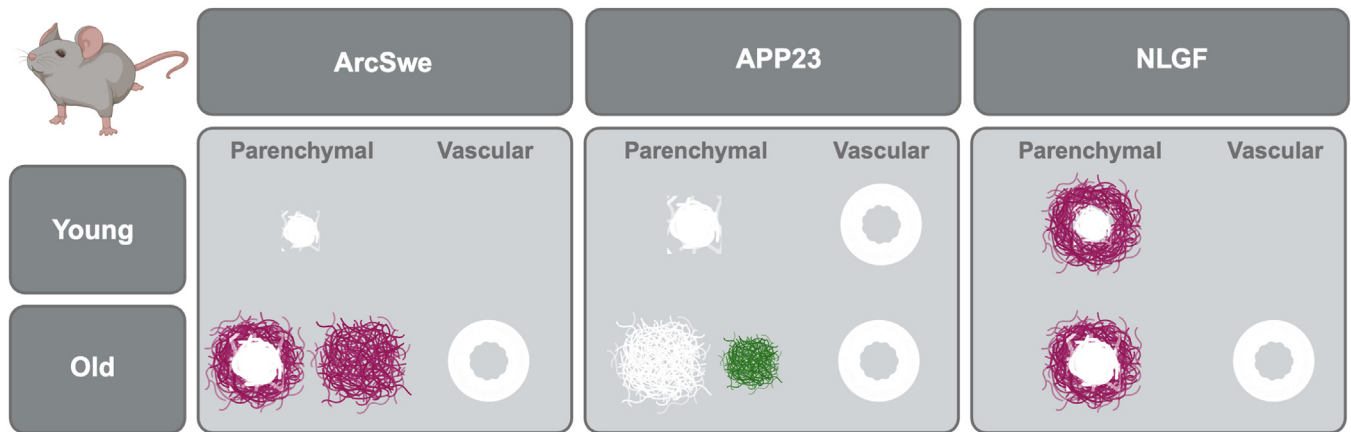


Figure 4. Schematic presentation of different parenchymal and vascular A β deposits that were identified with the dual-ligand staining protocols in mouse brain tissue sections. A β deposits identified by all five ligands are shown in white, whereas aggregated A β species solely identified by HS-84 and HS-169 or HS-259 are shown in magenta (HS-84 and HS-169) or green (HS-259). Different ligand staining patterns were observed for each mouse model. In APP^{ArcSwe} and APP23, age-related parenchymal A β deposits that were solely identified by HS-84 and HS-169 (APP^{ArcSwe}) or HS-259 (APP23) could be observed. The figure was created with BioRender.com. A β , amyloid- β ; APP, amyloid-beta precursor protein.

(Fig. 5G) and cored A β plaques (Fig. 5H). However, for the CAA lesions, the fluorescence from the respective ligand was only partly overlapping. A similar phenomenon was observed for A β assemblies in the white matter (Fig. S30). Most of these A β deposits were solely stained by HS-169, but some of the deposits also displayed HS-276 fluorescence. Moreover, the A β deposits in the gray matter that only showed HS-276 fluorescence had an appearance similar to the structures denoted as diffuse plaques in sAD (Fig. 5I), whereas the round aggregates that were lacking a core and solely displayed HS-169 fluorescence resembled CWP (Fig. 5J). Within a few of these assemblies, minor amounts of HS-276 fluorescence could also be observed (Fig. 5J). In cases from individuals with the Arctic APP mutation, the ligands showed strikingly different staining patterns (Figs. 5K and S29). For the A β plaques resembling CWP, which are hereafter referred to as cotton wool-like plaques, a term previously used for these types of deposits in cases with the Arctic APP mutation (57, 58), as well as aggregated tau pathologies, only HS-169 fluorescence was observed, whereas CAA lesions were stained by both ligands (Fig. 5, L–O). For the latter, the HS-276 fluorescence was rather weak and only partially overlapping with the fluorescence from HS-169. Immunohistochemistry (6E10 antibody) confirmed that HS-169 was labeling cotton wool-like A β plaques to some extent, and that these A β deposits were negative for HS-276 (Fig. S31). Overall, the experiments verified that the dual-ligand staining protocol comprised of HS-276 and HS-169 could be used to assign diverse types of A β deposits in different types of AD, since distinct ligand staining patterns were observed for the respective AD type. In sAD, HS-276 stained A β deposits were most abundant, whereas the opposite, HS-169 stained A β aggregates, were mainly observed in diAD associated with the Arctic mutation (APP E693G). Moreover, in diAD associated with the PSEN1 A431E mutation, a laminar staining pattern of the ligands was displayed (Fig. 5).

Variations in the ligand staining patterns for the sAD and diAD cases could also be observed when using the ligand

combination HS-84/HS-259 (Figs. 6 and S32). As reported previously for the individual ligands in sAD (43, 44), CAA lesions (Fig. 6B) and cored A β plaques (Fig. 6C) exhibited strong fluorescence from both ligands, whereas diffuse A β plaques (Fig. 6D) and white matter deposits (Fig. 6E) were only stained by HS-84. Both ligands also recognized tau aggregates. When examining brain tissue sections from individuals with the PSEN1 A431E mutation, a remarkable difference was seen compared to sAD, since only HS-84 staining was observed from the A β deposits (Figs. 6F and S32). CAA lesions (Fig. 6G), cored A β plaques (Fig. 6H), CWP (Fig. 6I), and white matter A β deposits (Fig. S33) displayed strong HS-84 fluorescence. Moreover, the diffuse A β aggregates that solely displayed HS-276 staining when using the protocol comprised of HS-276/HS-169, showed weaker HS-84 fluorescence compared to the other types of HS-84 positive A β deposits (Fig. 6J). Similar to the observation in sAD, tau aggregates were stained by both ligands. For the second type of diAD cases (Arctic E693G APP mutation), both ligands labeled cotton wool-like A β plaques, CAA lesions and tau aggregates (Fig. 6, L–O). HS-259 displayed intense fluorescence from both cotton wool-like A β plaques and tau aggregates, however, as previously reported for sAD (44), HS-259 showed distinct spectral signatures from these aggregates (Fig. S34). As confirmed with the 6E10 antibody, HS-259 fluorescence was observed from the majority of the cotton wool-like plaques that were identified by immunohistochemistry, whereas HS-84, in a similar fashion as HS-169, only labeled these aggregated A β species to some extent (Fig. S31). Compared to the CAA lesions, cotton wool-like A β plaques showed less intense HS-84 fluorescence, but in close vicinity to these deposits, some fibrillar A β aggregates that only displayed strong HS-84 fluorescence could be observed (Fig. 6O). Taken together, the observations from the HS-84 and HS-259 staining experiments, verified that this dual-ligand staining protocol could also be used to differentiate distinct A β deposits found in sAD or different types of diAD. HS-84 showed labeling of all A β deposit types in sAD and in diAD associated with the PSEN1 A431E mutation but limited

Chronological and spatial assignment of amyloid- β deposits

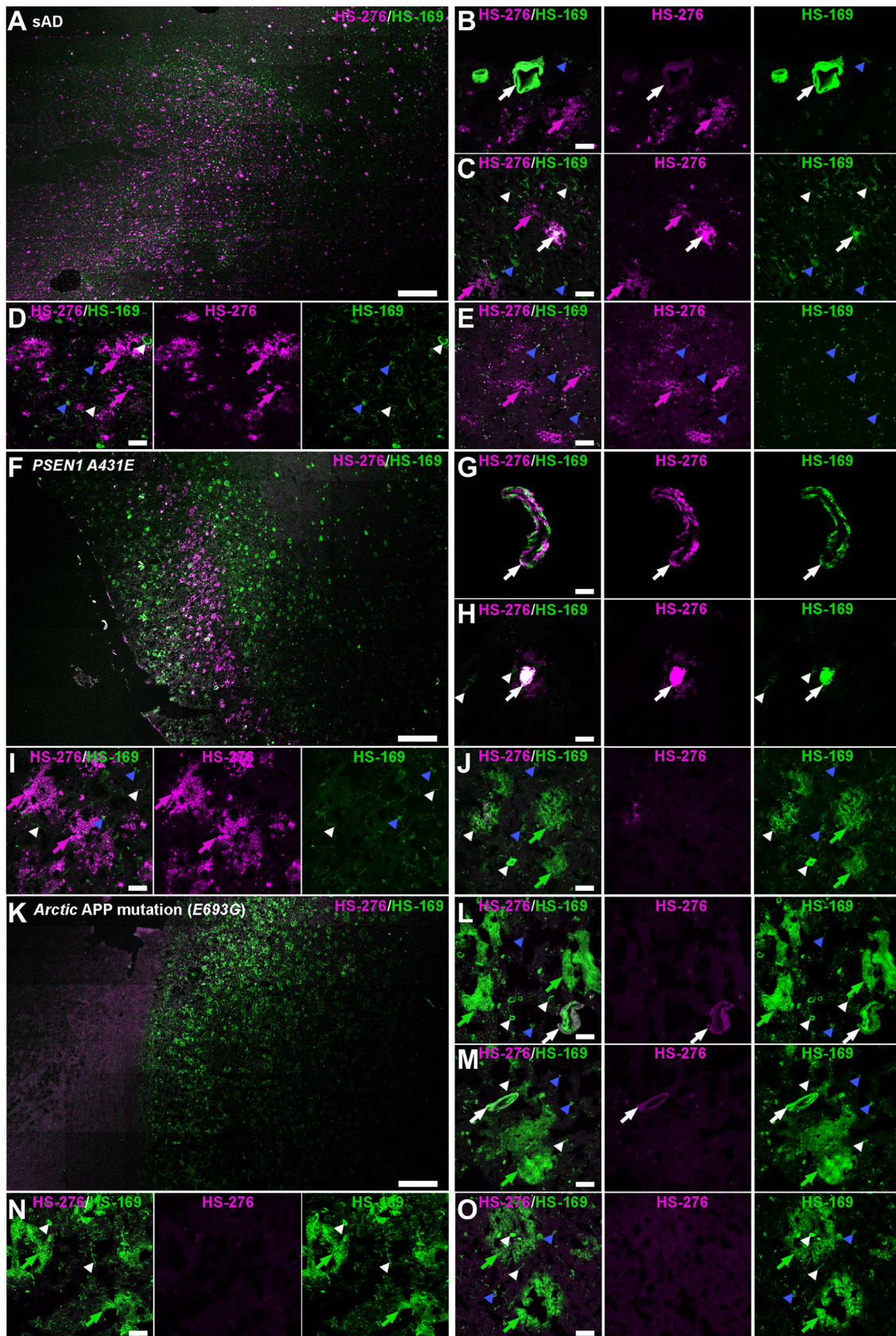


Figure 5. Dual-staining of human brain tissue sections (frontal cortex) from individuals with sAD or diAD with ligands HS-276 and HS-169. *A*, overview tile image of a brain tissue section from an individual with sAD. *B–E*, images of different A β aggregates, including CAA lesions (*B*), cored (*C*), and diffuse (*D*) A β plaques, as well as A β deposits in the white matter (*E*). *F*, overview tile image of a brain tissue section from an individual with diAD associated with the *PSEN1 A431E* mutation. *G–J*, images of different A β deposits, including CAA lesions (*G*), cored (*H*) and diffuse A β plaques (*I*), and cotton wool (*J*). *K*, overview tile image of a brain tissue section from an individual with Arctic APP mutation (*E693G*). *L–O*, images of different A β aggregates, including CAA lesions (*L*), cored (*M*) and diffuse A β plaques (*N*), as well as A β deposits in the white matter (*O*). White arrows point to specific A β aggregates, blue and green arrows indicate the localization of HS-276 and HS-169, respectively. White arrowheads point to diffuse A β plaques. Scale bars are shown in the bottom right of each panel.

staining in *APP E693G* cases. HS-259, on the other hand, displayed restricted labeling of A β aggregates in sAD and failed to detect A β in *PSEN1 A431E* tissue but showed strong labeling of A β deposits in *APP E693G* samples.

To validate the observations from the first two sets of ligand combinations, staining protocols comprised of HS-84/HS-169 or HS-276/HS-259 were next evaluated on the AD brain tissue sections (Figs. 7, 8, S35 and S36). In sAD, the same aggregates were identified by HS-84 or HS-169 fluorescence (Fig. 7, B–E), as when these ligands were used in combination with HS-259 or HS-276, respectively. Fluorescence from both ligands was detected from CAA lesions, cored A β plaques, and tau aggregates, whereas diffuse A β plaques and A β deposits in the white matter were only stained by HS-84. CAA lesions and cored A β plaques in *PSEN1 A431E* brain tissue sections also showed fluorescence from both ligands (Fig. 7, G and H). However, in contrast to previous observations for HS-169 when used in combination with HS-276, HS-169 staining of diffuse A β aggregates, CWPs, and A β aggregates in the white matter was lacking (Figs. 7, I and J, S37). Thus, in a similar fashion as for fibrillar A β deposits in *APP^{NL-G-F/NL-G-F}* mice (Fig. S16), for certain A β deposits in the *PSEN1 A431E* brain tissue sections, HS-84 was preventing binding of HS-169. This finding was also confirmed when using solely HS-169 for staining of *PSEN1 A431E* brain tissue sections, since bright fluorescence correlating to HS-169 could then be observed from diffuse A β aggregates, CWPs, and A β aggregates in the white matter (Fig. S38). For the Arctic mutation, the same ligand staining pattern was observed as with the previous protocols (Fig. 7, K–O). The cotton wool-like A β plaques, CAA lesions, and tau aggregates displayed fluorescence from both ligands, but again some fibrillar A β aggregates that solely displayed strong HS-84 fluorescence was observed nearby the cotton wool-like A β plaques (Fig. 7N).

When using the combination of HS-276 and HS-259, the same staining pattern was observed as when using each ligand in combination with HS-169 or HS-84, respectively. In sAD brain tissue sections, HS-276 fluorescence was observed from all A β deposits, whereas HS-259 only stained CAA lesions, cored A β plaques, and tau aggregates (Figs. 8, A–E and S36). Likewise, HS-276 stained all A β deposits except CWPs in *PSEN1 A431E* brain tissue sections and HS-259 was only observed from tau aggregates (Fig. 8, F–J). For the Arctic *APP* mutation cases, HS-276 fluorescence was lacking from all A β deposits except CAA lesions, whereas HS-259 staining was observed from cotton wool-like A β plaques, CAA lesions and tau aggregates (Fig. 8, K–O). With the two additional staining protocols, HS-335/HS-169 and HS-335/HS-259, similar staining patterns were observed as when using HS-276 instead of HS-335 (Figs. S39–S43). However, in contrast to HS-276, HS-335 fluorescence was also observed from some of the

6E10 positive cotton wool-like plaques in the Arctic cases (Figs. S31, S40, K–O and S42, K–O). Overall, the analysis of brain tissue sections from different AD types showed that dual-staining protocols comprised of two different ligands can be applied to identify distinct A β aggregates by fluorescence microscopy, since different ligand staining patterns were observed for the respective type of AD.

HS-276 and HS-259 display different staining patterns in brain tissue sections from different brain regions in individuals with sAD

The histological assessment of brain tissue sections from the same region, frontal cortex, clearly showed that the dual-staining protocols could be used to identify distinct A β deposits in individuals with sAD or diAD (Figs. 5–8). Therefore, one of the dual-staining protocols, HS-276/HS-259, was next used on tissue sections from different brain regions, frontal or visual cortex, from individuals with sAD. As shown above, in frontal cortex, the A β pathology was mainly labeled by HS-276, whereas HS-259 only labeled CAA lesions and cored A β plaques (Figs. 8 and S36). When comparing the staining pattern of frontal and visual cortex from three different individuals with sAD, a striking difference was observed between the regions, as the visual cortex displayed a larger amount of HS-259 fluorescence (Figs. 9A and S44). In the gray matter of visual cortex, the dominating A β deposits had a granular and diffuse appearance and only displayed bright HS-259 fluorescence. Some of these aggregates partially colocalized with fibrillar A β deposits that was solely stained by HS-276 (Fig. 9B). Both types of deposits were positive for the 6E10 A β antibody (Fig. S45), and the A β deposits also contained HS-259 positive tau aggregates that displayed a different emission spectrum than the A β deposits (Fig. S46). Furthermore, most of the HS-259 positive A β aggregates in the gray matter were negative for CN-PiB (Fig. S47). Similar to the observations in frontal cortex, the A β aggregates in the visual cortex white matter only displayed fluorescence from HS-276. Taken together, the distinct staining patterns displayed by HS-276 and HS-259 when comparing the results for frontal and visual cortex within the same sAD patient showed that the dual-staining protocol could be used to detect distinct types of A β deposits in different regions of the brain.

Discussion

From a diagnostic and therapeutic perspective, A β aggregates are central molecular targets in AD. Several ligands enabling clinical diagnostics by PET imaging have been presented (25, 59, 60), and recent reports of monoclonal antibodies stimulating the clearance of A β deposits from the brain have verified that these pathological species might be used as

plaques (J). K, overview tile image of a brain tissue section from an individual with diAD caused by the Arctic *APP E693G* mutation. L–O, images of different A β deposits, including CAA lesions (L and M) and cotton wool-like plaques (L–O). A β deposits stained by both ligands are indicated by white arrows, whereas A β aggregates only stained by HS-276 or HS-169 are highlighted with magenta (HS-276) or green (HS-169) arrows, respectively. Tau aggregates are indicated by white arrow heads and autofluorescence from granular lipofuscin is indicated by blue arrow heads. The staining was performed using 200 nM of the respective ligand in phosphate buffered saline (PBS, pH 7.4). Scale bars represent 500 μ m (A, F, and K) and 20 μ m (B–E, G–J, and L–O). A β , amyloid- β ; sAD: sporadic Alzheimer's disease; APP, amyloid-beta precursor protein; CAA, cerebral amyloid angiopathy; diAD, dominantly inherited AD; PSEN1, presenilin-1.

Chronological and spatial assignment of amyloid- β deposits

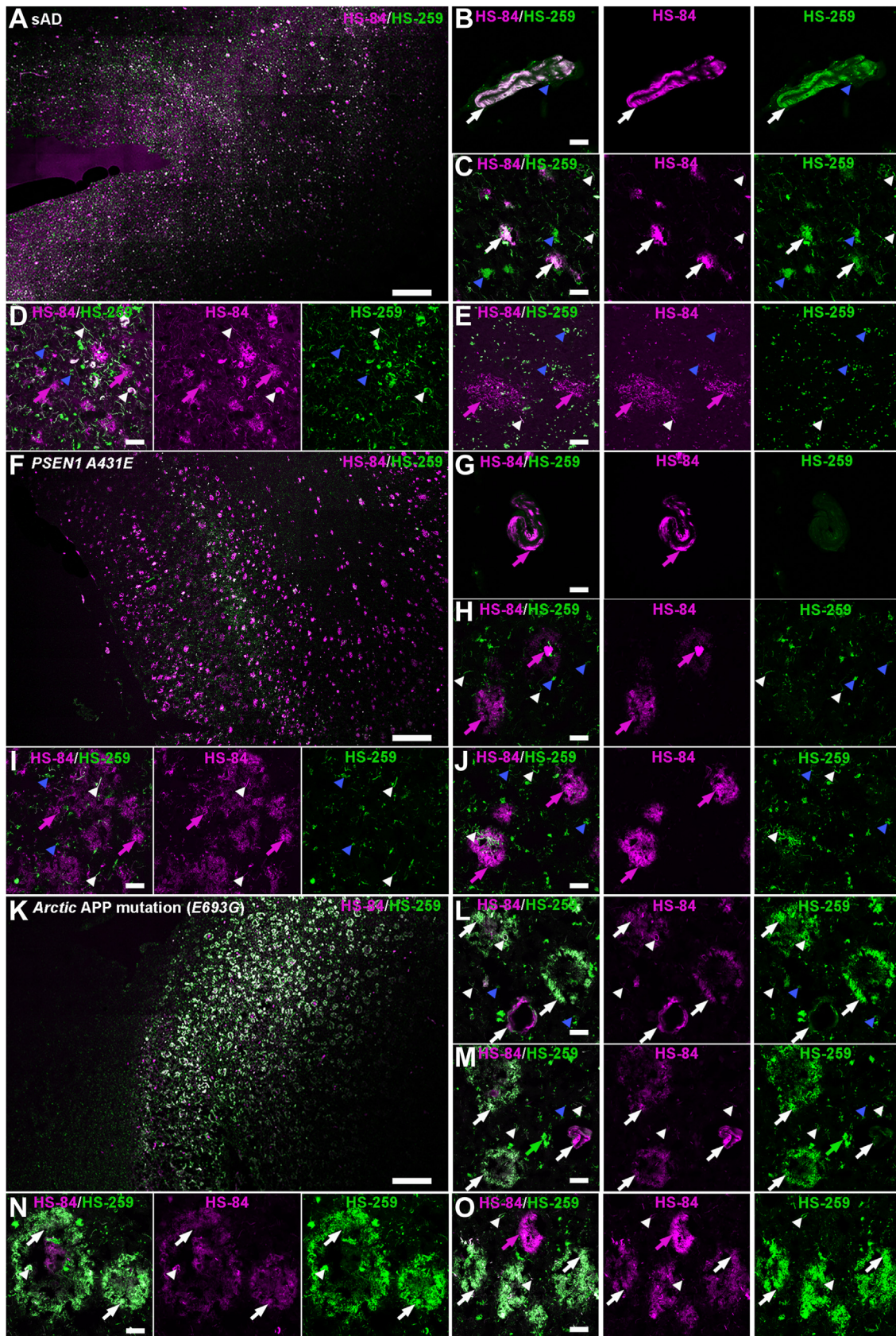


Figure 6. Dual-staining of human brain tissue sections (frontal cortex) from individuals with sAD or diAD with ligands HS-84 and HS-259. A, overview tile image of a brain tissue section from an individual with sAD. B–E, images of different aggregated A β pathologies, including CAA lesions (B), cored (C), diffuse (D), and A β deposits in the white matter (E). F, overview tile image of a brain tissue section from an individual with diAD associated with the *PSEN1* A431E mutation. G–J, images of different A β deposits, including CAA lesions (G), cored (H), and diffuse A β plaques (I), and cotton wool plaques (J).

targets for disease-modifying treatment for AD (61–63). However, the clinical benefit achieved in these trials has been rather modest (61–63), and PET tracers have shown limitation in detecting different A β deposits (26–28). Thus, a greater understanding of the presence of distinct A β deposits during the AD continuum and the pathogenesis of the disease is essential. Evidently, as several distinct folds of A β filaments (18–23), and also different variants of A β peptides (64–66), have been identified in AD, the existence of multiple types of A β deposits is highly likely. Therefore, it would be desirable to expand the methodologies available for the assignment of distinct A β deposits, and as shown herein, dual-staining protocols comprised of ligands with distinct photophysical characteristics and alternative binding modes offer a rather straightforward and simple approach for chronological and spatial histological assessment of different A β aggregates in brain tissue sections.

By using six variants of dual-staining protocols, different A β deposits could be assigned in brain tissue sections from APP mouse models and individuals with sAD or diAD with fluorescence microscopy (Figs. 4 and 10). In mouse brain sections, specific ligand staining patterns could be observed for the different mouse models, as well as for mice at different ages within each model (Fig. 4). The latter has also been observed when using a combination of a tetrameric oligothiophene, q-FTAA, and a heptameric oligothiophene, h-FTAA (32, 36). Within these studies, spectral analysis showed that the core of the A β deposits in young APPS1 and APP23 mice mainly displayed h-FTAA fluorescence whereas q-FTAA staining only was seen from the core of A β plaques in older mice (32, 36). In line with the results previously reported for q-FTAA (32, 36), HS-335 and HS-276 partially stained the core of larger A β plaques in old APP_{ArcSwe} and APP23 mice, but in young APP_{ArcSwe} and APP23 mice, the A β aggregates were identified by all five ligands (Fig. 4). Likewise, in young and old APP^{NL-G-F/NL-G-F}, the cored A β plaques were stained by all five ligands. However, in these mice, fibrillar A β aggregates solely labeled by HS-84 and HS-169 were also observed. In addition, A β aggregates only stained by HS-84 and HS-169 or HS-259 were observed in old APP_{ArcSwe} and APP23 mice, respectively (Fig. 4). Thus, in mouse models, the newly developed dual-ligand protocols seemed to identify an alternative range of A β aggregates than the previously reported protocol comprised of q-FTAA and h-FTAA. Dual-staining protocols comprised of other fluorescent amyloid ligands have also been used to show a variation in A β deposits in 5xAD mice (38, 40), but a comparison of aggregates in mice of different ages was lacking in these studies. Lately, a rather comprehensive methodology, using multiple spectral collection from aggregates stained by a single ligand followed by principal component analysis of the data, also showed a difference between A β

aggregates in transgenic mouse models (41). The q-FTAA/h-FTAA protocol has also been used for evaluating temporal and spatial efficacy of anti-A β therapies in transgenic mice (67), and we foresee that the dual-staining protocols described herein can be used in a similar fashion. Furthermore, two of the ligands, HS-84 and HS-169, included in this study have also been used for longitudinal *in vivo* imaging of protein aggregates by multiphoton microscopy (68). Hence, applying dual-ligand staining protocols for real time assignment of distinct A β deposits in mouse models is an additional tantalizing possibility.

Distinct ligand staining patterns could also be observed on brain tissue sections from individuals with sAD or diAD associated with the *PSEN1 A431E* mutation (51–53) or the Arctic *APP E693G* mutation (54, 55) (Fig. 10). For sAD, the observed ligand staining patterns agreed with earlier studies when the respective ligands were used (42–45), whereas alternative ligand staining patterns were displayed from A β deposits in the diAD cases. Firstly, laminar staining patterns with distinct fluorescence were seen in the *PSEN1 A431E* cases and diffuse A β plaques displayed intense fluorescence from HS-276 and HS-335, as well as weaker emission from HS-84 and HS-169, whereas CWP were solely detected by HS-84 and HS-169. In an earlier study, CWP were readily identified with X-34, a fluorescent analogue of Congo red, but poorly stained by CN-PiB (31). Hence, in agreement with our results, ligands that share the same binding mode as Congo red, such as HS-84 and HS-169, recognize CWP. Furthermore, in a recent study, CWP were detected by the heptameric oligothiophenes, h-FTAA and LL-1 (69), whereas the HS-276 positive diffuse A β plaques were readily labeled by CN-PiB, as well as h-FTAA. Secondly, in contrast to the other ligands, HS-259 did not bind to any types of A β deposits in the *PSEN1 A431E* brain tissue sections except occasionally weak staining of the core of cored plaques. However, a strikingly intense HS-259 fluorescence was observed from the cotton wool-like plaques in the Arctic *APP* mutation cases. These A β plaques have been shown to be negative for Congo red and thioflavin S (57, 58), as well as for carbon-11 labeled Pittsburgh compound-B, [11C]PiB (70), but were to some extent labeled by the other ligands included in our study. Hence, the CWP in the *PSEN1 A431E* cases and the cotton wool-like plaques in the Arctic *APP* mutation cases displayed differential staining patterns by the fluorescent ligands. Strikingly different ligand staining patterns were also observed with HS-276/HS-259 when comparing different brain regions from individuals with sAD (Fig. 10), indicating that the dual-staining protocols can be used for gaining novel findings regarding the role and presence of distinct A β deposits during the AD pathogenesis. From a histopathological perspective, it would be of great interest to compare the ligand staining patterns in individuals

K, overview tile image of a brain tissue section from an individual with diAD caused by the Arctic *APP E693G* mutation. L–O, images of different A β deposits, including CAA lesions (L and M) and cotton wool-like plaques (L–O). A β deposits stained by both ligands are indicated by white arrows, whereas A β aggregates only stained by HS-84 or HS-259 are highlighted with magenta (HS-84) or green (HS-259) arrows, respectively. Tau aggregates are indicated by white arrow heads and autofluorescence from granular lipofuscin is indicated by blue arrow heads. The staining was performed using 200 nM of the respective ligand in phosphate buffered saline (PBS, pH 7.4). Scale bars represent 500 μ m (A, F, and K) and 20 μ m (B–E, G–J and L–O). A β , amyloid- β ; sAD: sporadic Alzheimer's disease; CAA, cerebral amyloid angiopathy; APP, amyloid-beta precursor protein; diAD, dominantly inherited AD; PSEN1, presenilin-1.

Chronological and spatial assignment of amyloid- β deposits

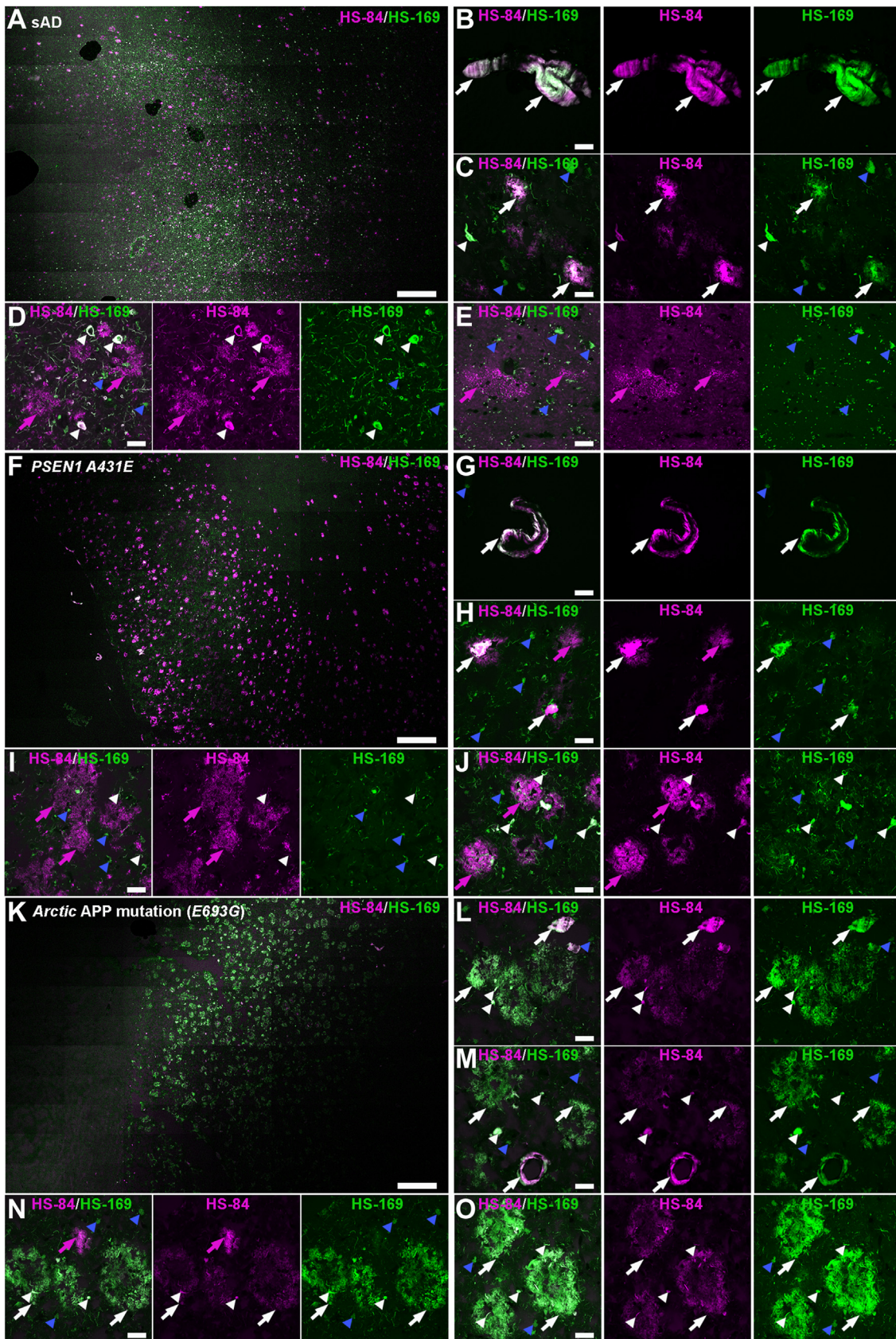


Figure 7. Dual-staining of human brain tissue sections (frontal cortex) from individuals with sAD or diAD with ligands HS-84 and HS-169. A, overview tile image of a brain tissue section from an individual with sAD. B–E, images of different A β deposits, including CAA lesions (B), cored (C), diffuse (D), and A β aggregates in the white matter (E). F, overview tile image of a brain tissue section from an individual with diAD associated with the *PSEN1 A431E* mutation. G–J, images of different A β deposits, including CAA lesions (G), cored (H), and diffuse A β plaques (I) and cotton wool plaques (J). K, overview tile

with different disease progression, onset of disease or clinical symptoms, as well as analyzing several brain regions from the same individual. Another appealing possibility is to use the dual-staining protocols in proteopathic seed amplification assays, since it was recently reported that a single thiophene-based ligand could be used to discriminate between samples of cerebrospinal fluid from patients diagnosed with Parkinson's disease and samples from patients with multiple system atrophy (71). A seed amplification assay has also been used to detect A β in cerebrospinal fluid samples from AD patients (72), and by combining this technology with the dual-ligand staining methodology, novel insights regarding the properties of the A β aggregates in AD patients might be afforded. For clinical imaging by PET, further chemical evolution of the ligands is required since ligands similar to HS-84 and HS-169 have shown very low brain uptake when converted to PET tracers (73). On the other hand, PET tracers based on the HS-259 molecular scaffold might be of great interest, since this ligand stained the cotton wool-like plaques in the Arctic *APP* mutation cases, as well as the CN-PiB negative aggregated A β pathologies in the visual cortex from individuals with sAD.

Clearly, the binding mode for a certain thiophene-based ligand is only accessible on distinct A β deposits and several studies have shown that minor modifications of the molecular structure of the ligand can have a substantial impact on its ability to identify certain aggregated proteins (33, 39, 42–46). From a biological perspective, the detection of distinct A β deposits by a specific thiophene-based ligand has been correlated to a certain composition of specific A β peptides within the aggregates (36, 69). Thus, specific binding modes of distinct ligands can be afforded due to a particular content of A β peptides within the deposit and previous studies have shown that the main component of the HS-84 and HS-169 positive CWP in *PSEN1 A431E* individuals are amino-terminally truncated A β peptide species, such as the pyroglutamate-modified A β peptides A β 3pE-42 and A β 11pE-42 (56, 69). Distinct contents of modified A β peptides have also been reported for A β deposits in cases with the Arctic *APP* mutation (57, 58). In these studies (57, 58), a variation of A β peptides were observed within the same deposits, as well as between different deposits. This variation might alter the ligand binding mode, since HS-84, HS-169 and HS-335 only labeled a fraction of the A β aggregates identified by 6E10, whereas HS-259 fluorescence was observed from the majority of the deposits. Differential binding modes might also be obtained due to different structures of the A β filaments within the deposits. As shown by cryo-EM, the fold of A β 42 filaments in sAD individuals (type I fold) was different than the fold of A β 42 filaments in diAD individuals (type II fold) (19), and a distinct fold was also reported for A β filaments with the Arctic *APP* mutation (20). Our findings show some correlation with these folds, since HS-276

staining was predominantly observed in sAD (type I fold) whereas the staining of cotton wool-like plaques in the Arctic *APP* mutation cases was lacking. However, with fluorescence microscopy, structural information regarding A β deposits can only be obtained within the micrometer to submicrometer domain, whereas with cryo-EM, resolution in the Ångström range can be achieved. Thus, to compare observations obtained by the respective technique, correlative imaging, in a similar fashion as used to relate ligand staining to A β peptide content (36, 69), is necessary. Cryogenic correlated light and electron tomography, using the amyloid ligand methoxy-X04 to resolve the in-tissue molecular architecture of A β deposits in the brain of transgenic mice, was recently presented (74), and we foresee that our ligand dual-staining protocols can be used in a similar fashion to identify protein aggregates that subsequently can be assessed by electron microscopy. Evidently, the dual-staining protocols can be used to assign distinct types of A β deposits in different brain regions, and in combination with cryo-EM, spatial resolution of distinct A β aggregates down to an atomic level might be feasible.

In conclusion, we have shown that dual-staining protocols comprised of different ligands with different binding modes and photophysical properties can be used for chronological and spatial histological assignment of distinct A β deposits by fluorescence microscopy. Our discoveries demonstrate the importance of using multiple ligands for obtaining a precise assignment of different A β deposits. The latter would be highly relevant from a clinical perspective, as well as for the precise evaluation of therapeutic agents targeting A β aggregates, and we foresee that our findings can aid in developing novel tools for resolving these matters.

Experimental procedures

Mouse brain tissue sections

All experimental procedures were approved by the Uppsala County Animal Ethics board (5.8.18–20,401/2020) and the Swedish Ethical Review Authority (Dnr 2020–01197, 2020–06–25), carried out according to the regulations of the Swedish Animal Welfare Agency, and complied with the European Communities Council Directive of 22 September 2010 (2010/63/E.U.). All mouse models were maintained on a C57BL/6 background. The APP^{ArcSwe} mice, harboring the Arctic (*APP E693G*) and Swedish (*APPKM670/671NL*) mutations, show elevated levels of soluble A β protofibrils already at a very young age and abundant and rapidly developing plaque pathology, forming plaques that resemble those found in sAD (22), starting at around 6 months of age (48). APP^{NL-G-F/NL-G-F} mice, expressing mouse APP with a humanized A β sequence and with the Swedish (*KM670/671NL*), Arctic (*E693G*), and Iberian (*I716F*) *APP* mutations show A β deposits as early as 3 to

image of a brain tissue section from an individual with diAD caused by the Arctic *APP E693G* mutation. L–O, images of different A β deposits, including CAA lesions (L and M) and cotton wool-like plaques (L–O). A β deposits stained by both ligands are indicated by white arrows, whereas A β aggregates only stained by HS-84 or HS-169 are highlighted with magenta (HS-84) or green (HS-169) arrows, respectively. Tau aggregates are indicated by white arrow heads and autofluorescence from granular lipofuscin is indicated by blue arrow heads. The staining was performed using 200 nM of the respective ligand in phosphate buffered saline (PBS, pH 7.4). Scale bars represent 500 μ m (A, F, and K) and 20 μ m (B–E, G–J and L–O). A β , amyloid- β ; sAD: sporadic Alzheimer's disease; diAD, dominantly inherited AD; CAA, cerebral amyloid angiopathy; APP, amyloid-beta precursor protein; PSEN1, presenilin-1.

Chronological and spatial assignment of amyloid- β deposits

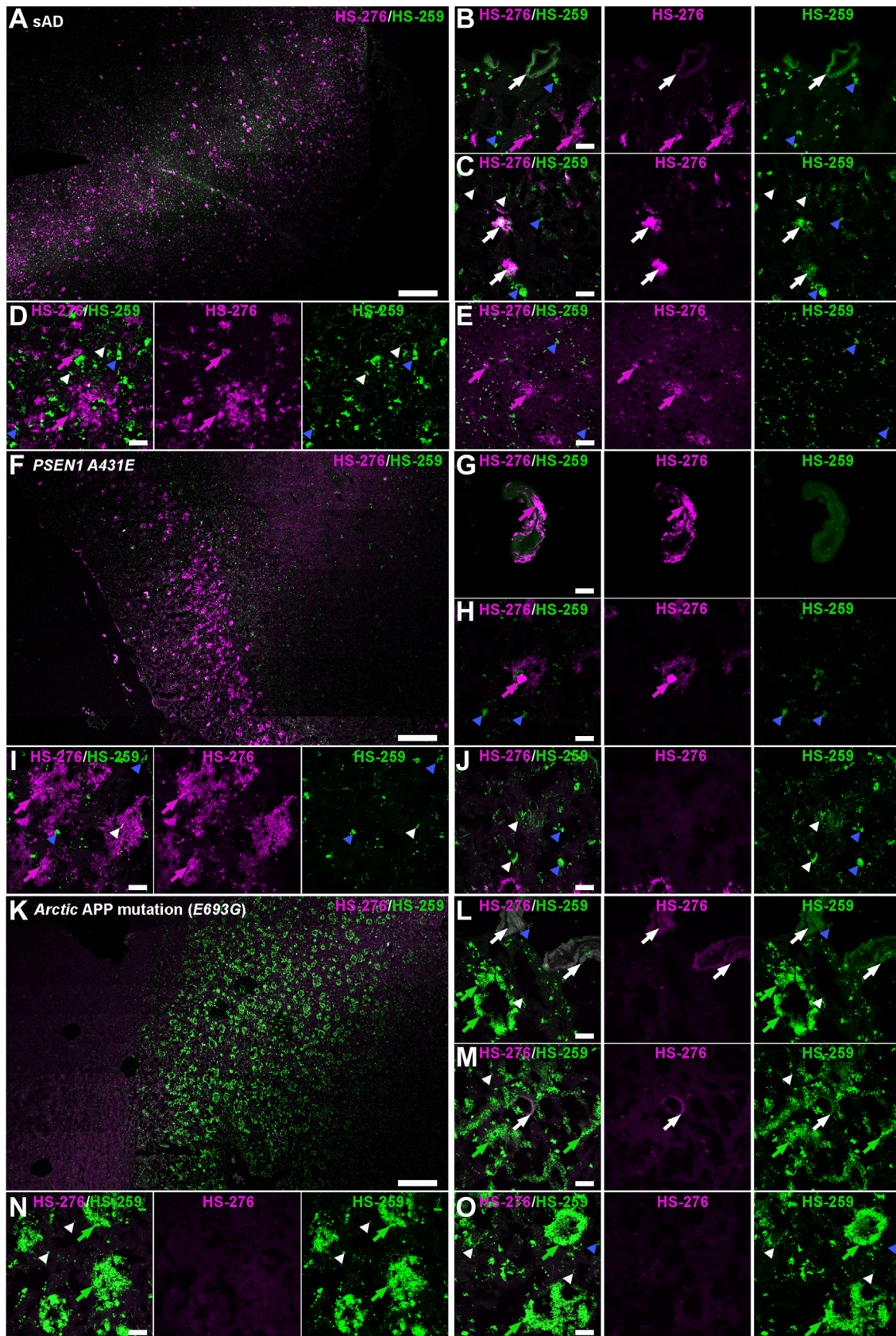


Figure 8. Dual-staining of human brain tissue sections (frontal cortex) from individuals with sAD or diAD with ligands HS-276 and HS-259. *A*, overview tile image of a brain tissue section from an individual with sAD. *B–E*, images of different A β deposits, including CAA lesions (*B*), cored (*C*), diffuse (*D*), and A β aggregates in the white matter (*E*). *F*, overview tile image of a brain tissue section from an individual with diAD associated with the *PSEN1 A431E* mutation. *G–J*, images of different A β deposits, including CAA lesions (*G*), cored (*H*), and diffuse A β plaques (*I*), and cotton wool plaques (*J*). *K*, overview tile

4 months of age consisting of predominantly A β 42 (49). APP23 mice have a 7-fold overexpression of human A β PP with the Swedish mutation (KM670/671NL) and produce more A β 40 than A β 42, as well as show deposits around 6 months of age (47). In the study, frozen brain tissue samples from APP_{ArcSwe} (n = 6), APP^{NL-G-F/NL-G-F} (n = 6) and APP23 (n = 4) transgenic mice with two different ages from each model (Table S1) were included. The experiments were performed on 10 μ m thick sections from frozen brain tissue samples.

Human brain tissue sections

This study was performed in line with the principles of the Declaration of Helsinki. The collection of *post mortem* human brain tissue and their use in this project were reviewed and approved by the Regional Ethical Committee in Uppsala, Sweden and the Swedish Ethical Review Authority (Dnr 2005–244; Dnr 2020–01197; Dnr 2021–04766; 2011/962–31/1), as well as the Indiana University Institutional Review Board. For all cases, informed consent was obtained from the patient or their next of kin. In the study, frozen brain tissue samples from individuals diagnosed with sAD (n = 5) or diAD associated with the *PSEN1 A431E* (n = 3) or the *APP E693G* (Arctic) (n = 2) mutation were included. For sAD, the analyses were carried out on brain samples collected from frontal (n = 5) or visual (n = 3) cortex. For diAD, brain samples from frontal cortex (n = 5) were analyzed. The experiments were performed on 10 μ m thick sections of the included frozen brain tissue samples.

Staining of brain tissue sections with different combinations of ligands

The synthesis of thiophene-based ligands HS-84 (42, 43), HS-169 (43), HS-259 (44), HS-335 (44), and HS-276 (45) has been reported previously. The ligands were dissolved in deionized water (HS-84 and HS-169) or dimethyl sulfoxide (HS-259, HS-276, and HS-335) to a final concentration of 1.5 mM. Prior to histological staining, these stock solutions were diluted to a final concentration of 200 nM of the respective ligand in phosphate buffered saline (PBS, 10 mM phosphate, 140 mM NaCl, 2.7 mM KCl, pH 7.4). Staining solutions comprised of ligand combinations HS-84/HS-259, HS-84/HS-169, HS-276/HS-169, HS-276/HS-259, HS-335/HS-169, or HS-335/HS-259 were prepared. Frozen brain tissue sections (10 μ m) were fixed in 99.7% EtOH for 10 min at room temperature (RT), incubated 10 min in 50% EtOH followed by 10 min in deionized water at RT and then 10 min in PBS. The sections were incubated with the respective staining solution (200 nM of each ligand in PBS) for 30 min at RT. The sections were then washed with PBS three times and mounted with Dako mounting medium for fluorescence (Agilent). The mounting medium was allowed to solidify at least overnight

before sealing the cover slips with nail polish. In addition to the combination staining experiments, consecutive brain sections from APP^{NL-G-F} mouse (18 months old) or a diAD patient with the *PSEN1 A431E* mutation were also stained with only HS-84 or HS-169 (200 nM) using the same procedure as for the dual-staining protocol.

Ligand and antibody double staining

Frozen brain tissue sections (10 μ m) were fixed in prechilled 70% EtOH for 3 min at 4 °C and then incubated 2 \times 2 min in dH₂O, 10 min in PBS, and 1 h in PBS with 0.1% Triton x-100 and 5% normal goat serum (blocking buffer) at RT. Anti-A β antibody 6E10 (BioLegend) was diluted 1:1000 in blocking buffer and added to the sections. After incubation over night at 4 °C, the sections were washed 3 \times 10 min in PBS with 0.1% Triton x-100 and then incubated for 1 h at RT with goat anti-mouse secondary antibody conjugated with Alexa Fluor 488/594/647 (Thermo Fisher Scientific) diluted 1:500 in blocking buffer. After washing in PBS, the sections were incubated with the ligand staining solution (200 nM ligand in PBS) as described above. The sections were then washed with PBS three times and mounted with Dako mounting medium for fluorescence (Agilent). The mounting medium was allowed to solidify at least overnight before sealing the cover slips with nail polish.

HS-259 staining together with q-FTAA/h-FTAA or CN-PiB

Staining solutions comprised of HS-259 (200 nM)/q-FTAA (120 nM)/h-FTAA (256 nM) or HS-259 (200 nM)/CN-PiB (1 μ M) were prepared in PBS. Frozen brain tissue sections (10 μ m) were fixed in 99.7% EtOH for 10 min at RT, incubated 10 min in 50% EtOH followed by 10 min in deionized water at RT and then 10 min in PBS. The sections were incubated with the respective staining solution for 30 min at RT. The sections were then washed with PBS three times and mounted with Dako mounting medium for fluorescence (Agilent). The mounting medium was allowed to solidify at least overnight before sealing the cover slips with nail polish.

Fluorescence microscopy

The sections were analyzed using an inverted Zeiss LSM 780 laser scanning confocal microscope (Zeiss) using the following channel set up for each ligand:

HS-276:	Excitation: 405 nm	Emission: 455 to 547 nm
HS-335:	Excitation: 405 nm	Emission: 463 to 547 nm
HS-84:	Excitation: 490 nm	Emission: 495 to 572 nm
HS-169:	Excitation: 565 nm	Emission: 585 to 712 nm
HS-259:	Excitation: 565 nm	Emission: 585 to 712 nm

image of a brain tissue section from an individual with diAD caused by the Arctic *APP E693G* mutation. L–O, images of different A β deposits, including CAA lesions (L and M) and cotton wool-like plaques (L–O). A β deposits stained by both ligands are indicated by *white arrows*, whereas A β aggregates only stained by HS-276 or HS-259 are highlighted with *magenta* (HS-276) or *green* (HS-259) *arrows*, respectively. Tau aggregates are indicated by *white arrow heads* and autofluorescence from granular lipofuscin is indicated by *blue arrow heads*. The staining was performed using 200 nM of the respective ligand in phosphate buffered saline (PBS, pH 7.4). Scale bars represent 500 μ m (A, F, and K) and 20 μ m (B–E, G–J, and L–O). A β , amyloid- β ; sAD, sporadic Alzheimer's disease; diAD, dominantly inherited AD; CAA, cerebral amyloid angiopathy; APP, amyloid-beta precursor protein; PSEN1, presenilin-1.

Chronological and spatial assignment of amyloid- β deposits

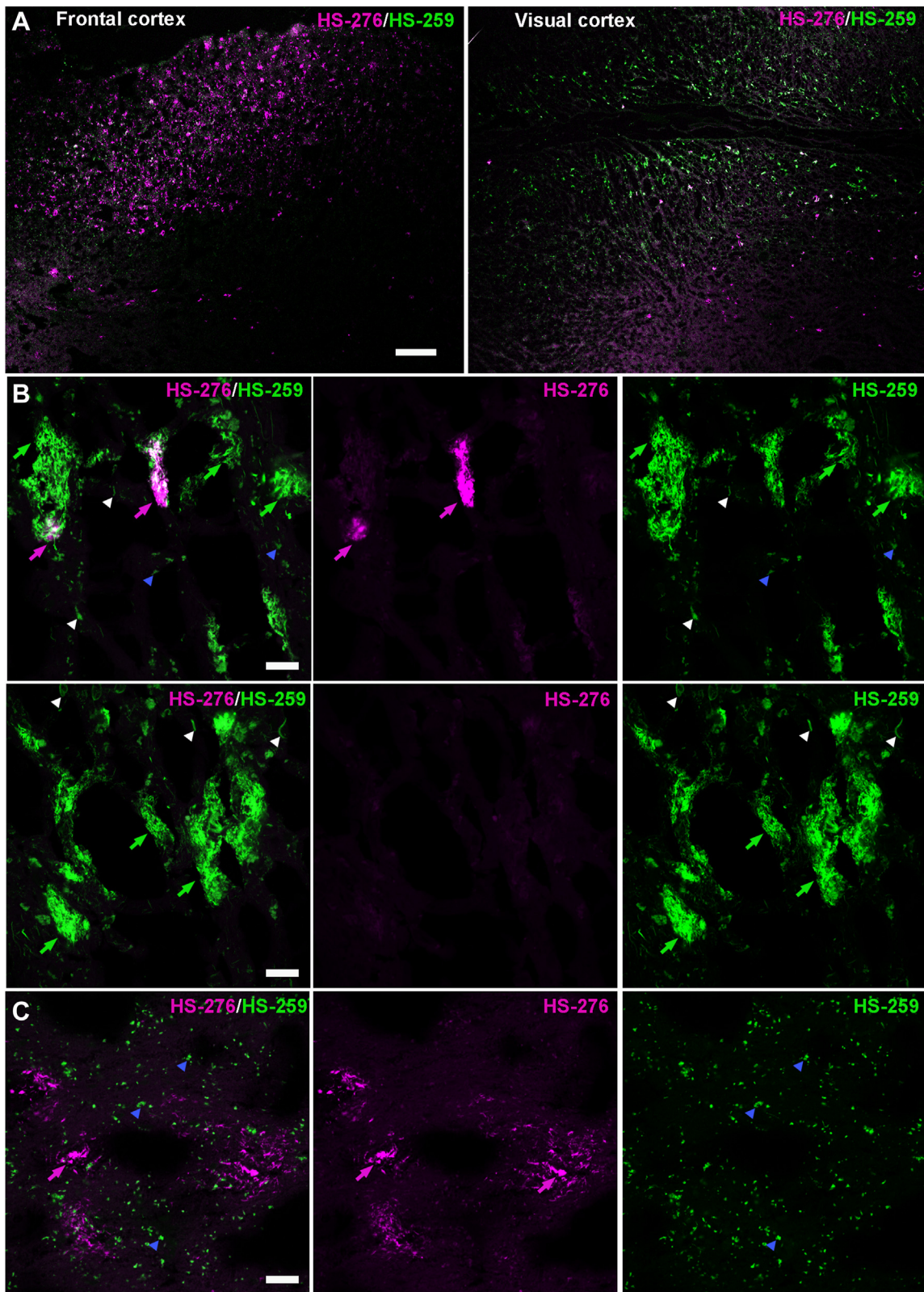


Figure 9. Images of human brain tissue sections, collected from frontal or visual cortex, from an individual with sAD, stained with a dual-staining protocol comprised of ligands HS-276 and HS-259. *A*, overview tile image of brain tissue sections from frontal (*left*) or visual (*right*) cortex. *B* and *C*, images of different A β deposits in the gray (*B*) or white (*C*) matter region of visual cortex. A β deposits only stained by HS-276 or HS-259 are highlighted with magenta (HS-276) or green (HS-259) arrows, respectively. Tau aggregates are indicated by white arrow heads and autofluorescence from granular lipofuscin is indicated by blue arrow heads. The staining was performed using 200 nM of the respective ligand in phosphate buffered saline (PBS, pH 7.4). Scale bars represent 500 μ m (*A*) and 20 μ m (*B* and *C*). A β , amyloid- β ; sAD: sporadic Alzheimer's disease.

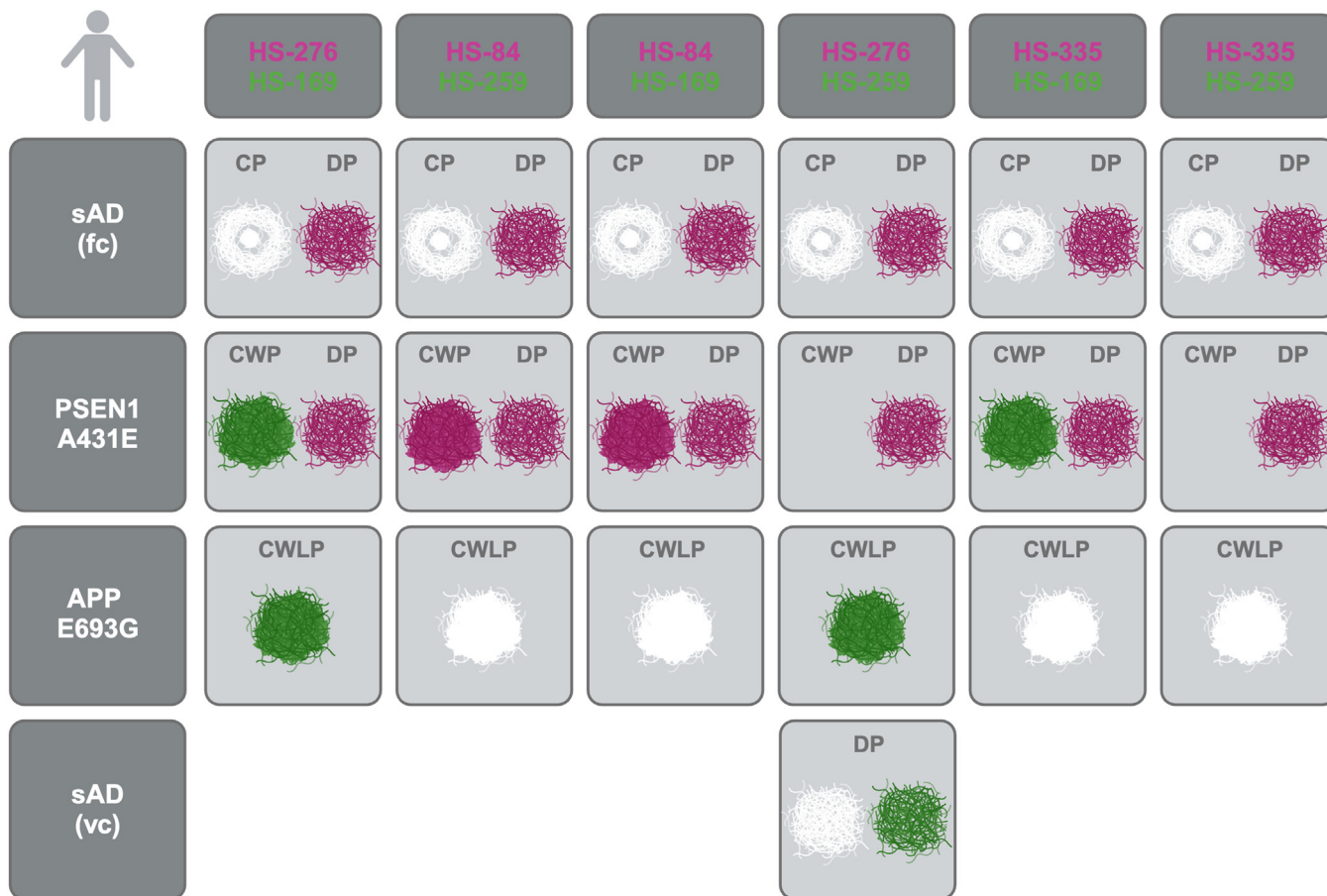


Figure 10. Schematic presentation of different parenchymal Ab deposits that were identified with each dual-ligand staining protocols in human brain tissue sections. Parenchymal A β deposits, such as cored plaques (CP), diffused plaques (DP), cotton wool plaques (CWP), and cotton wool like plaques (CWLP) identified by both ligands are shown in *white*, whereas A β deposits solely identified by one of the ligands are shown in *magenta* (HS-276, HS-84, or HS-335) or *green* (HS-169 and HS-259). Distinct ligand staining patterns were observed between different types of AD, as well as between different brain regions, frontal cortex (fc), and visual cortex (vc) in sporadic AD (sAD). The figure was created with [BioRender.com](https://www.biorender.com). A β , amyloid- β ; AD, Alzheimer's disease.

For HS-259 bound to A β and tau pathologies, full emission spectra were also collected using an excitation at 565 nm.

Data availability

The data discussed in this study are presented in the manuscript and supporting information. Source data and additional data can be obtained from the corresponding author upon reasonable request.

Supporting information—This article contains supporting information.

Acknowledgments—We thank Xiongyu Wu for the synthesis of CN-PiB and the Linköping University core facilities at the faculty for Medical and Health Sciences and the faculty for Science and Engineering (ProLinC) for technical support and instrument access.

Author contributions—T. K., F. P., and K. P. R. N. investigation; T. K., R. V., B. G., D. S., S. S., and K. P. R. N. conceptualization; T. K., and K. P. R. N. methodology; T. K. and K. P. R. N. visualization; T.

K., and K. P. R. N. validation; T. K. and K. P. R. N. formal analysis; T. K. and K. P. R. N. writing—original draft; H. S., F. P., S. N., P. H., C. G., M. I., R. V., B. G., D. S., and S. S. writing—review and editing; H. S., S. N., P. H., C. G., M. I., R. I., B. G., D. S., and S. S. resources; S. N., P. H., and K. P. R. N. funding acquisition; P. H. resources; K. P. R. N. supervision; K. P. R. N. project administration.

Funding and additional information—This work was supported by the US National Institutes of Health (2RF1NS110437-06 (R. V., B. G., and K. P. R. N.)), the Swedish Research Council (2016-00748 (K. P. R. N.), 2021-01083 (S. S.), 2021-03524 (D. S.), 2023-03275 (K. P. R. N.), 2023-03931 (P. H.)), the Swedish Brain Foundation (FO2022-0072 (K. P. R. N.), FO2020-0207 (P. H. and S. N.), ALZ2019-0004 (P. H. and S. N.), and ALZ2022-0004 (P. H. and S. N.)) and Gustav V and Drottning Viktorias Foundation (P. H.). The content is solely the responsibility of the authors and does not necessarily represent the official views of the National Institutes of Health.

Conflict of interest—The authors declare that they have no conflicts of interest with the contents of this article.

Abbreviations—The abbreviations used are: A β , amyloid- β ; AD, Alzheimer's disease; CAA, cerebral amyloid angiopathy; CWP,

Chronological and spatial assignment of amyloid- β deposits

cotton wool plaque; diAD, dominantly inherited Alzheimer's disease; PSEN1, presenilin-1; sAD, sporadic Alzheimer's disease; PiB, Pittsburgh compound-B; RT, room temperature.

References

1. Alzheimer, A. (1907) Über eine eigenartige Erkrankung der Hirnrinde. *Allg. Z. Psychiatr.* **64**, 146–148
2. Glenner, G. G., and Wong, C. W. (1984) Alzheimer's disease: initial report of the purification and characterization of a novel cerebrovascular amyloid protein. *Biochem. Biophys. Res. Commun.* **120**, 885–890
3. Masters, C. L., Simms, G., Weinman, N. A., Multhaup, G., McDonald, B. L., and Beyreuther, K. (1985) Amyloid plaque core protein in Alzheimer disease and Down syndrome. *Proc. Natl. Acad. Sci. U. S. A.* **82**, 4245–4249
4. Grundke-Iqbal, I., Iqbal, K., Quinlan, M., Tung, Y. C., Zaidi, M. S., and Wisniewski, H. M. (1986) Microtubule-associated protein tau. A component of Alzheimer paired helical filaments. *J. Biol. Chem.* **261**, 6084–6089
5. Joachim, C. L., Duffy, L. K., Morris, J. H., and Selkoe, D. J. (1988) Protein chemical and immunocytochemical studies of meningeovascular β -amyloid protein in Alzheimer's disease and normal aging. *Brain Res.* **474**, 100–111
6. Prelli, F., Castaño, E., Glenner, G. G., and Frangione, B. (1988) Differences between vascular and plaque core amyloid in Alzheimer's disease. *J. Neurochem.* **51**, 648–651
7. Iwatsubo, T., Odaka, A., Suzuki, N., Mizusawa, H., Nukina, N., and Ihara, Y. (1993) Visualization of A β 42(43) and A β 40 in senile plaques with end-specific A β monoclonals: evidence that an initially deposited species is A β 42(43). *Neuron* **13**, 45–53
8. Miller, D. L., Papayannopoulos, I. A., Styles, J., Bobin, S. A., Lin, Y. Y., Biemann, K., et al. (1993) Peptide compositions of the cerebrovascular and senile plaque core amyloid deposits of Alzheimer's disease. *Arch. Biochem. Biophys.* **301**, 41–52
9. Mann, D. M. A., Iwatsubo, T., Ihara, Y., Cairns, N. J., Lantos, P. L., Bogdanovic, N., et al. (1996) Predominant deposition of amyloid- β 42(43) in plaques in cases of Alzheimer's disease and hereditary cerebral hemorrhage associated with mutations in the amyloid precursor protein gene. *Am. J. Pathol.* **148**, 1257–1266
10. Gkanatsiou, E., Portelius, E., Toomey, C. E., Blennow, K., Zetterberg, H., Lashley, T., et al. (2019) A distinct brain beta amyloid signature in cerebral amyloid angiopathy compared to Alzheimer's disease. *Neurosci. Lett.* **701**, 125–131
11. Petkova, A. T., Leapman, R. D., Guo, Z., Yau, W.-M., Mattson, M. P., and Tycko, R. (2005) Self-propagating, molecular-level polymorphism in Alzheimer's β -Amyloid Fibrils. *Science* **307**, 262–265
12. Paravastu, A. K., Leapman, R. D., Yau, W.-M., and Tycko, R. (2008) Molecular structural basis for polymorphism in Alzheimer's beta-amyloid fibrils. *Proc. Natl. Acad. Sci. U. S. A.* **105**, 18349–18354
13. Sachse, C., Fändrich, M., and Grigorieff, N. (2008) Paired beta-sheet structure of an Abeta(1-40) amyloid fibril revealed by electron microscopy. *Proc. Natl. Acad. Sci. U. S. A.* **105**, 7462–7466
14. Schmidt, M., Rohou, A., Lasker, K., Yadav, J. K., Schiene-Fischer, C., Fändrich, M., et al. (2015) Peptide dimer structure in an A β (1-42) fibril visualized with cryo-EM. *Proc. Natl. Acad. Sci. U. S. A.* **112**, 11858–11863
15. Gremer, L., Schölzel, D., Schenk, C., Reinartz, E., Labahn, J., Ravelli, R. B. G., et al. (2017) Fibril structure of amyloid- β (1-42) by cryo-electron microscopy. *Science* **358**, 116–119
16. Lu, J.-X., Qiang, W., Yau, W.-M., Schwieters, C. D., Meredith, S. C., and Tycko, R. (2013) Molecular structure of β -amyloid fibrils in Alzheimer's disease brain tissue. *Cell* **154**, 1257–1268
17. Qiang, W., Yau, W.-M., Lu, J.-X., Collinge, J., and Tycko, R. (2017) Structural variation in amyloid- β fibrils from Alzheimer's disease clinical subtypes. *Nature* **541**, 217–221
18. Kollmer, M., Close, W., Funk, L., Rasmussen, J., Bsoul, A., Schierhorn, A., et al. (2019) Cryo-EM structure and polymorphism of A β amyloid fibrils purified from Alzheimer's brain tissue. *Nat. Commun.* **10**, 4760
19. Yang, Y., Arseni, D., Zhang, W., Huang, M., Lövestam, S., Schweighauser, M., et al. (2022) Cryo-EM structures of amyloid- β 42 filaments from human brains. *Science* **375**, 167–172
20. Yang, Y., Zhang, W., Murzin, A. G., Schweighauser, M., Huang, M., Lövestam, S., et al. (2023) Cryo-EM structures of amyloid- β filaments with the Arctic mutation (E22G) from human and mouse brains. *Acta Neuropathol.* **145**, 325–333
21. Yang, Y., Murzin, A. G., Peak-Chew, S., Franco, C., Garringer, H. J., Newell, K. L., et al. (2023) Cryo-EM structures of A β 40 filaments from the leptomeninges of individuals with Alzheimer's disease and cerebral amyloid angiopathy. *Acta Neuropathol. Commun.* **11**, 191
22. Zielinski, M., Peralta Reyes, F. S., Gremer, L., Schemmert, S., Frieg, B., Schäfer, L. U., et al. (2023) Cryo-EM of A β fibrils from mouse models find tg-APP^{ArcSwe} fibrils resemble those found in patients with sporadic Alzheimer's disease. *Nat. Neurosci.* **26**, 2073–2080
23. Scheres, S. H. W., Ryskeldi-Falcon, B., and Goedert, M. (2023) Molecular pathology of neurodegenerative diseases by cryo-EM of amyloids. *Nature* **621**, 701–710
24. Nilsson, K. P. R. (2013) Small organic probes as amyloid specific ligands—past and recent molecular scaffolds. *EMBO Rep.* **14**, 1017–1022
25. Klunk, W. E., Engler, H., Nordberg, A., Wang, Y., Blomqvist, G., Holt, D. P., et al. (2004) Imaging brain amyloid in Alzheimer's disease with Pittsburgh Compound-B. *Ann. Neurol.* **55**, 306–319
26. Ikonovic, M. D., Klunk, W. E., Abrahamson, E. E., Mathis, C. A., Price, J. C., Tsopelas, N. D., et al. (2008) Post-mortem correlates of in vivo PiB-PET amyloid imaging in a typical case of Alzheimer's disease. *Brain* **131**, 1630–1645
27. Svedberg, M. M., Hall, H., Hellström-Lindh, E., Estrada, S., Guan, Z., Nordberg, A., et al. (2009) [11C] PiB-amyloid binding and levels of A β 40 and A β 42 in postmortem brain tissue from Alzheimer patients. *Neurochem. Int.* **54**, 347–357
28. Rosen, R. F., Ciliax, B. J., Wingo, T. S., Gearing, M., Dooyema, J., Lah, J. J., et al. (2010) Deficient high-affinity binding of Pittsburgh compound B in a case of Alzheimer's disease. *Acta Neuropathol.* **119**, 221–233
29. Crook, R., Verkkoniemi, A., Perez-Tur, J., Mehta, N., Baker, M., Houlden, H., et al. (1998) A variant of Alzheimer's disease with spastic paraparesis and unusual plaques due to deletion of exon 9 of presenilin 1. *Nat. Med.* **4**, 452–455
30. Maarouf, C. L., Daus, I. D., Spina, S., Vidal, R., Kokjohn, T. A., Patton, R. L., et al. (2008) Histopathological and molecular heterogeneity among individuals with dementia associated with Presenilin mutations. *Mol. Neurodegener.* **3**, 20
31. Abrahamson, E. E., Kofler, J. K., Becker, C. R., Price, J. C., Newell, K. L., Ghetti, B., et al. (2021) 11C-PiB PET can underestimate brain amyloid- β burden when cotton wool plaques are numerous. *Brain* **145**, 2161–2176
32. Nyström, S., Psonka-Antonczyk, K. M., Ellingsen, P. G., Johansson, L. B. G., Reitan, N., Handrick, S., et al. (2013) Evidence for age-dependent in vivo conformational rearrangement within A β amyloid deposits. *ACS Chem. Biol.* **8**, 1128–1133
33. Klingstedt, T., Shirani, H., Mahler, J., Wegenast-Braun, B. M., Nyström, S., Goedert, M., et al. (2015) Distinct spacing between anionic groups: an essential chemical determinant for achieving thiophene-based ligands to distinguish β -amyloid or tau polymorphic aggregates. *Chemistry* **21**, 9072–9082
34. Rasmussen, J., Mahler, J., Beschoner, N., Kaeser, S. A., Häsler, L. M., Baumann, F., et al. (2017) Amyloid polymorphisms constitute distinct clouds of conformational variants in different etiological subtypes of Alzheimer's disease. *Proc. Natl. Acad. Sci. U. S. A.* **114**, 13018–13023
35. Condello, C., Lemmin, T., Stöhr, J., Nick, M., Wu, Y., Maxwell, A. M., et al. (2018) Structural heterogeneity and intersubject variability of A β in familial and sporadic Alzheimer's disease. *Proc. Natl. Acad. Sci. U. S. A.* **115**, E782–E791
36. Michno, W., Nyström, S., Wehrli, P., Lashley, T., Brinkmalm, G., Guerard, L., et al. (2019) Pyroglutamation of amyloid- β x-42 (A β x-42) followed by A β 1-40 deposition underlies plaque polymorphism in progressing Alzheimer's disease pathology. *J. Biol. Chem.* **294**, 6719–6732

37. Maxwell, A. M., Yuan, P., Rivera, B. M., Schaaf, W., Mladinov, M., Prasher, V. P., *et al.* (2021) Emergence of distinct and heterogeneous strains of amyloid beta with advanced Alzheimer's disease pathology in Down syndrome. *Acta Neuropathol. Commun.* **9**, 201
38. Stepanchuk, A. A., Morgan, M. L., Joseph, J. T., and Stys, P. K. (2022) Dual-probe fluorescence spectroscopy for sensitive quantitation of Alzheimer's amyloid pathology. *Acta Neuropathol. Commun.* **10**, 153
39. Lantz, L., Shirani, H., Ghetti, B., Vidal, R., Klingstedt, T., and Nilsson, K. P. R. (2023) Thiophene-based ligands for histological multiplex spectral detection of distinct protein aggregates in Alzheimer's disease. *Chemistry* **29**, e202203568
40. Stepanchuk, A. A., and Stys, P. K. (2023) Amyloid dye pairs as spectral sensors for enhanced detection and differentiation of misfolded proteins. *J. Photochem. Photobiol. B.* **248**, 112786
41. Yang, H., Yuan, P., Wu, Y., Shi, M., Caro, C. D., Tengeji, A., *et al.* (2023) EMBER multidimensional spectral microscopy enables quantitative determination of disease- and cell-specific amyloid strains. *Proc. Natl. Acad. Sci. U. S. A.* **120**, e2300769120
42. Simon, R. A., Shirani, H., Åslund, K. O. A., Bäck, M., Haroutunian, V., Gandy, S., *et al.* (2014) Pentameric thiophene-based ligands that spectrally discriminate amyloid- β and tau aggregates display distinct solvatochromism and viscosity-induced spectral shifts. *Chemistry* **20**, 12537–12543
43. Shirani, H., Linares, M., Sigurdson, C. J., Lindgren, M., Norman, P., and Nilsson, K. P. R. (2005) A palette of fluorescent thiophene-based ligands for the identification of protein aggregates. *Chemistry* **21**, 15133–15137
44. Björk, L., Shirani, H., Todarwal, Y., Linares, M., Vidal, R., Ghetti, B., *et al.* (2023) Distinct heterocyclic moieties govern the selectivity of thiophene-vinylene-based ligands towards A β or tau pathology in Alzheimer's disease. *Eur. J. Org. Chem.* **26**, e2023005
45. Klingstedt, T., Shirani, H., Ghetti, B., Vidal, R., and Nilsson, K. P. R. (2021) Thiophene-based optical ligands that selectively detect A β pathology in Alzheimer's disease. *Chembiochem.* **22**, 2568–2581
46. Herrmann, U. S., Schütz, A. K., Shirani, H., Huang, D., Saban, D., Nuvolone, M., *et al.* (2015) Structure-based drug design identifies polythiophenes as antiprion compounds. *Sci. Transl. Med.* **7**, 299ra123
47. Sturchler-Pierrat, C., Abramowski, D., Duke, M., Wiederhold, K. H., Mistl, C., Rothacher, S., *et al.* (1997) Two amyloid precursor protein transgenic mouse models with Alzheimer disease-like pathology. *Proc. Natl. Acad. Sci. U. S. A.* **94**, 13287–13292
48. Lord, A., Kalimo, H., Eckman, C., Zhang, X. Q., Lannfelt, L., and Nilsson, L. N. (2006) The Arctic Alzheimer mutation facilitates early intraneuronal Abeta aggregation and senile plaque formation in transgenic mice. *Neurobiol. Aging* **27**, 67–77
49. Saito, T., Matsuba, Y., Mihira, N., Takano, J., Nilsson, P., Itoharu, S., *et al.* (2014) Single App knock-in mouse models of Alzheimer's disease. *Nat. Neurosci.* **17**, 661–663
50. Baghallab, I., Reyes-Ruiz, J. M., Abulnaja, K., Huwait, E., and Glabe, C. (2018) Epitomic characterization of the specificity of the anti-amyloid A β monoclonal antibodies 6E10 and 4G8. *J. Alzheimers Dis.* **66**, 1234–1244
51. Rogueva, E. A., Fafel, K. C., Song, Y. Q., Medeiros, H., Sato, C., Liang, Y., *et al.* (2001) Screening for PS1 mutations in a referral-based series of AD cases: 21 novel mutations. *Neurology* **57**, 621–625
52. Yescas, P., Huertas-Vazquez, A., Villarreal-Molina, M. T., Rasmussen, A., Tusié-Luna, M. T., López, M., *et al.* (2006) Founder effect for the Ala431Glu mutation of the presenilin 1 gene causing early-onset Alzheimer's disease in Mexican families. *Neurogenetics* **7**, 195–200
53. Murrell, J., Ghetti, B., Cochran, E., Macias-Islas, M. A., Medina, L., Varpetian, A., *et al.* (2006) The A431E mutation in PSEN1 causing Familial Alzheimer's Disease originating in Jalisco state, Mexico: an additional fifteen families. *Neurogenetics* **7**, 277–279
54. Nilsberth, C., Westlind-Danielsson, A., Eckman, C. B., Condron, M. M., Axelman, K., Forsell, C., *et al.* (2001) The 'Arctic' APP mutation (E693G) causes Alzheimer's disease by enhanced A β protofibril formation. *Nat. Neurosci.* **4**, 887–893
55. Basun, H., Bogdanovic, N., Ingelsson, M., Almkvist, O., Näslund, J., Axelman, K., *et al.* (2008) Clinical and neuropathological features of the Arctic APP mutation causing early onset Alzheimer's disease. *Arch. Neurol.* **65**, 499–505
56. Miravalle, L., Calero, M., Takao, M., Roher, A. E., Ghetti, B., and Vidal, R. (2005) Amino-terminally truncated A β peptide species are the main component of cotton wool plaques. *Biochemistry* **44**, 10810–10821
57. Philipson, O., Lord, A., Lalowski, M., Soliymani, R., Baumann, M., Thyberg, J., *et al.* (2012) The Arctic amyloid- β precursor protein (A β PP) mutation results in distinct plaques and accumulation of N- and C-truncated A β . *Neurobiol. Aging* **33**, 1010.e1
58. Kalimo, H., Lalowski, M., Bogdanovic, N., Philipson, O., Bird, T. D., Nochlin, D., *et al.* (2013) The Arctic A β PP mutation leads to Alzheimer's disease pathology with highly variable topographic deposition of differentially truncated A β . *Acta Neuropathol. Commun.* **1**, 60
59. Nelissen, N., Van Laere, K., Thurfjell, L., Owenius, R., Vandenbulcke, M., Koole, M., *et al.* (2009) Phase 1 study of the Pittsburgh compound B derivative 18F-flutemetamol in healthy volunteers and patients with probable Alzheimer disease. *J. Nucl. Med.* **50**, 1251–1259
60. Vandenberghe, R., Van Laere, K., Ivanou, A., Salmon, E., Bastin, C., Triau, E., *et al.* (2010) 18F-flutemetamol amyloid imaging in Alzheimer disease and mild cognitive impairment: a phase 2 trial. *Ann. Neurol.* **68**, 319–329
61. Budd Haeblerlein, S., Aisen, P. S., Barkhof, F., Chalkias, S., Chen, T., Cohen, S., *et al.* (2022) Two randomized phase 3 studies of aducanumab in early Alzheimer's disease. *J. Prev. Alzheimers Dis.* **9**, 197–210
62. van Dyck, C. H., Swanson, C. J., Aisen, P., Bateman, R. J., Chen, C., Gee, M., *et al.* (2023) Lecanemab in early Alzheimer's disease. *N. Engl. J. Med.* **388**, 9–21
63. Sims, J. R., Zimmer, J. A., Evans, C. D., Lu, M., Ardayfio, P., Sparks, J., *et al.* (2023) Donanemab in early symptomatic Alzheimer disease: the TRAILBLAZER-ALZ 2 randomized clinical trial. *JAMA Netw. Open* **6**, e2323349
64. Maler, J. M., Klafki, H. W., Paul, S., Spitzer, P., Groemer, T. W., Henkel, A. W., *et al.* (2007) Urea-based two-dimensional electrophoresis of beta-amyloid peptides in human plasma: evidence for novel Abeta species. *Proteomics* **7**, 3815–3820
65. Guntert, A., Döbeli, H., and Bohrmann, B. (2006) High sensitivity analysis of amyloid-beta peptide composition in amyloid deposits from human and PS2APP mouse brain. *Neuroscience* **143**, 461–475
66. Portelius, E., Brinkmalm, G., Tran, A. J., Zetterberg, H., Westman-Brinkmalm, A., and Blennow, K. (2009) Identification of novel APP/Abeta isoforms in human cerebrospinal fluid. *Neurodegener. Dis.* **6**, 87–94
67. Kirschenbaum, D., Dadgar-Kiani, E., Catto, F., Voigt, F. F., Trevisan, C., Bichsel, O., *et al.* (2023) Whole-brain microscopy reveals distinct temporal and spatial efficacy of anti-A β therapies. *EMBO Mol. Med.* **15**, e16789
68. Calvo-Rodriguez, M., Hou, S. S., Snyder, A. C., Dujardin, S., Shirani, H., Nilsson, K. P. R., *et al.* (2019) In vivo detection of tau fibrils and amyloid β aggregates with luminescent conjugated oligothiophenes and multiphoton microscopy. *Acta Neuropathol. Commun.* **7**, 171
69. Klingstedt, T., Lantz, L., Shirani, H., Ge, J., Hanrieder, J., Vidal, R., *et al.* (2024) Thiophene-based ligands for specific assignment of distinct A β pathologies in Alzheimer's disease. *ACS Chem. Neurosci.* **15**, 1581–1595
70. Schöll, M., Wall, A., Thordardottir, S., Ferreira, D., Bogdanovic, N., Långström, B., *et al.* (2012) Low PiB PET retention in presence of pathologic CSF biomarkers in Arctic APP mutation carriers. *Neurology* **79**, 229–236
71. Shah Nawaz, M., Mukherjee, A., Pritzkow, S., Mendez, N., Rabadia, P., Liu, X., *et al.* (2020) Discriminating α -synuclein strains in Parkinson's disease and multiple system atrophy. *Nature* **578**, 273–277
72. Salvadores, N., Shah Nawaz, M., Scarpini, E., Tagliavini, F., and Soto, C. (2014) Detection of misfolded A β oligomers for sensitive biochemical diagnosis of Alzheimer's disease. *Cell Rep.* **7**, 261–268
73. Nordeman, P., Johansson, L. B. G., Bäck, M., Estrada, S., Hall, H., Sjölander, D., *et al.* (2016) (11)C and (18)F radiolabeling of tetra- and pentathiophenes as PET-ligands for amyloid protein aggregates. *ACS Med. Chem. Lett.* **7**, 368–373
74. Leistner, C., Wilkinson, M., Burgess, A., Lovatt, M., Goodbody, S., Xu, Y., *et al.* (2023) The in-tissue molecular architecture of β -amyloid pathology in the mammalian brain. *Nat. Commun.* **14**, 2833